Nanoparticle Size Effect on Some Magnetic Properties

19

Costica Caizer

Contents

Abstract

Nanoparticles exhibit, from a magnetic point of view, various anomalies and specific magnetic properties, different from those of the bulk with the same chemical composition. Knowing the new magnetic properties is very important, both from theoretical point of view and their numerous practical applications in nanotechnology (nanotechnics and, recently, in nanomedicine), which should be considered. In this chapter we shall present an overview on the following topics: saturation magnetization, magnetic anisotropy, and magnetic behavior of magnetic nanoparticles, in relation with their size and magnetic structure, single- or multi-domains. The magnetic properties of the nanoparticles are compared and discussed in relation to those of the corresponding bulk. The surface effects, in the case of surfacted nanoparticles and those embedded in different matrices, on

C. Caizer (✉)
West University of Timisoara, Faculty of Physics, Department of Physics, Timisoara, Romania
e-mail: ccaizer@physics.uvt.ro; costica.caizer@e-uvt.ro

M. Aliofkhazraei (ed.), *Handbook of Nanoparticles*,
DOI 10.1007/978-3-319-15338-4_24

magnetic properties are presented and discussed in the core–shell model (core of the nanoparticle, where the magnetic moments are aligned under the exchange interaction, and the shell, where the magnetic moments are in a disordered structure).

Keywords
Nanoparticles • Size effect • Saturation magnetisation • Magnetic anisotropy • Magnetic behaviour • Magnetic relaxation

Introduction

According to their size, the nanoparticles (NPs) are in the dimensional range: from a few nm until hundreds of nm (considering the diameter of the particles as a linear dimension (D), for the approximation of the spherical nanoparticles). The effect of their size is strongly reflected on the magnetic structure of nanoparticles and, consequently, on their magnetic behavior in an external magnetic field. By reducing the size of the nanoparticles from tens of nanometers to a few nanometers (Fig. 1), their magnetic structure changes: from a structure with magnetic domains ($D > D_c$, where D_c is the critical diameter), where the magnetization is stable and nonuniform (Weiss domains), to a structure without magnetic domains (single-domain structure) ($D_t < D < D_c$, where D_t is the threshold diameter), with stable and uniform magnetization or unstable magnetization (transition state), at very small dimensions ($D < D_t$), to a single-domain structure but with fluctuant magnetization along a direction in the crystal (easy magnetization axis) (superparamagnetic (SPM) range). The magnetic structures result from the condition of minimization of the free energy of the crystal, which leads to its stable configuration.

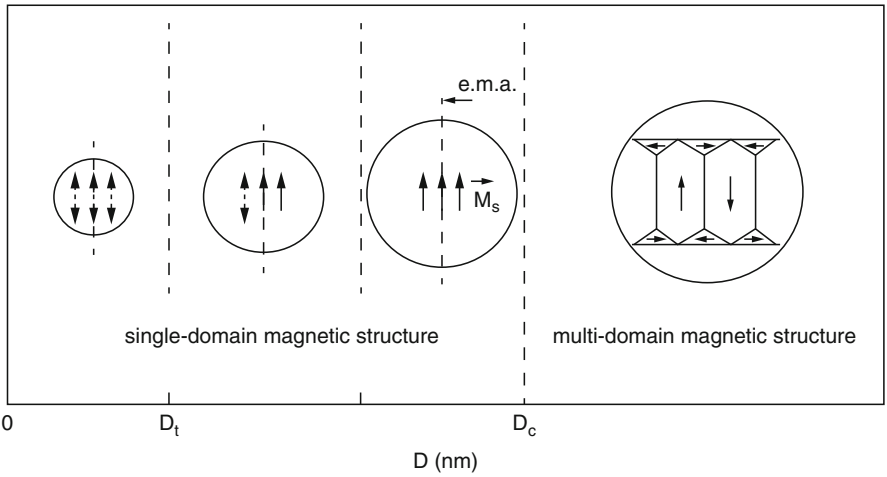

Fig. 1 The single- and multi-domain magnetic structures of nanoparticles

Table 1 Magnetization and magnetic behavior of nanoparticles according to their size and magnetic structures

Nanoparticle size (nm)	Magnetic structure	Magnetization state	Magnetic behavior	Basic reference[a]
$D > D_c$	Multi-domain	Stable nonuniform	Large hysteresis loop (like bulk)	[75, 98, 102]
$D_t << D < D_c$ (closer to D_c)	Single domain	Stable uniform	Hysteresis loop (from rectangular to linear)	[103–105, 107, 108, 110]
$D_t < D << D_c$ (closer to D_t)	Single domain	Transition state (relaxation)	Small hysteresis loop to no hysteresis	[102, 104, 114]
$0 < D < D_t$	Single domain	Fluctuating	Superparamagnetic	[33, 122–124, 127, 129, 139]

[a]In section "Magnetic Behavior of Nanoparticles in an External Field"

At small dimensions (usually a few nanometers), the magnetization of the single-domain nanoparticle is no longer stable, and it can reverse to 180° under the effect of the thermal activation. The transition state may be considered a *transition* area between the state of magnetic stability and the superparamagnetic state (SPM). The magnetic behavior of these nanostructures is with hysteresis ($D > D_t$) and anhysteretic ($D < D_t$), more precisely SPM (see subsection "Superparamagnetic Behavior of the Nanoparticles"), behavior which, at a given temperature, is also highly influenced by the magnetic anisotropy of NPs. These data are summarized in Table 1. The results obtained so far have shown that the saturation magnetization of NPs (Ms) depends on their size, the saturation magnetization reducing along with the reduction of the size, as a result of the spin disorder at the surface of the nanoparticles, which leads to a dominant effect at very small dimensions.

In this chapter, we present and discuss the effect of the size of nanoparticles on the saturation magnetization, magnetic anisotropy, magnetic structure, and magnetic behavior. The chapter is divided into three sections. The first section approaches the issue of *saturation magnetization of nanoparticles*, which, in general, *is lower than that of the corresponding bulk*; here, we take into account the spin disorder at the surface of the nanoparticles and the variation of the NP saturation magnetization with temperature, which is unusual, in many cases. The second section presents the magnetic anisotropy in the case of nanoparticles, which is generally *higher* (*much higher in some cases*) *than the magnetocrystalline anisotropy* of the bulk, which is dominated by *the surface anisotropy* in the case of very small nanoparticles, as it is shown by the results of many experiments. The last section presents the *behavior of the nanoparticles in an external magnetic field*, according to *their size*, which has a certain magnetic structure, resulted from the competition of the exchange, magnetostatic, and anisotropy forces.

The *size* of the nanoparticles, determined during the process of their obtaining or by some subsequent thermal treatments, is a *basic parameter* for many practical applications, in addition to the nature of the material; also, the shape and size

distribution of nanoparticles, as well as the magnetostatic interactions between them, can change the magnetic behavior of a system of nanoparticles. Moreover, using surfactants or covering the nanoparticles with a layer, or embedding them in different solid, noncrystalline, or crystalline matrices (nanocomposites) or their dispersion in a carrier liquid (nanofluids) can change the magnetic properties of the nanosystem. Knowing these aspects, and their effects on the magnetic behavior of nanoparticles in an external magnetic field, is very important from a practical point of view, for future applications in nanotechnology.

Here we will take into consideration these aspects in the case of nanoparticles with ferro- and ferrimagnetic ordering of their internal magnetic moments (due to the exchange interaction (direct) and, respectively, superexchange interaction (indirect, through the oxygen ions) of the magnetic moments). We will not discuss the case of antiferromagnetic, which can be found in other bibliographic references (chapters, books). Also, the effects described are discussed in the absence of interactions.

Saturation Magnetization of Nanoparticles

Surface Spin Disorder in Nanoparticles and Saturation Magnetization

Many results, both experimental and theoretical [1–6], have shown that the *saturation magnetization of nanoparticles* is lower than that of the corresponding bulk material and that it decreases rapidly along with decreasing the size of very small (nm) nanoparticles [7]. The magnetization ($\vec{M}$) of a material is determined by the resulting magnetic moment ($\vec{\mu}$) per unit volume (V). For an elementary volume, in the case of continuous distribution of magnetic (atomic) moments, the magnetization is

$$\vec{M} = \frac{d\vec{\mu}}{dV}, \tag{1}$$

the magnetization vector $\vec{M}$ having the same direction and sense as the elementary magnetic moment $d\ \vec{\mu}$. For a large-sized nanoparticle (tens to hundreds of nm) which has a magnetic domain structure, at magnetic saturation, all the magnetic atomic moments are on the same direction (the direction of the externally applied magnetic field), the magnetization of the nanoparticle being, in this case, uniform and equal to the saturation magnetization (spontaneous) (M_s) of the material. Under these conditions, according to Eq. 1, the magnetic moment for a volume of material will be

$$m = M_s \int_{(V)} dV, \tag{2}$$

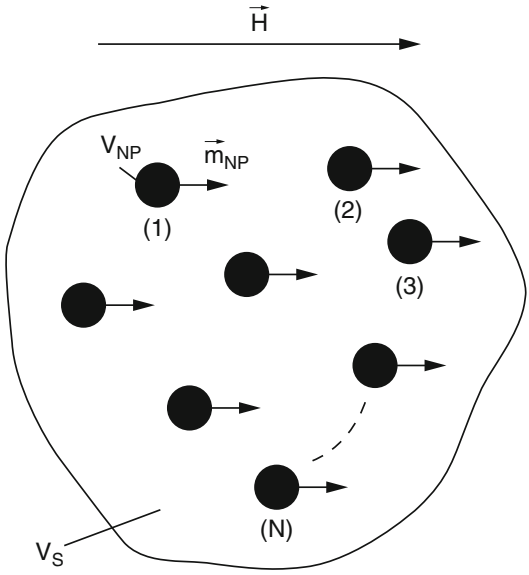

Fig. 2 System of nanoparticles without interaction at magnetic saturation

for the finite volume (known) of the particle (V_P),

$$m_P = M_s V_P. \tag{3}$$

In the case of *small* (nm to tens of nm), *single-domain nanoparticles* (without a structure of magnetic domains), their volume is generally smaller than a magnetic domain (Weiss domain), domain in which the magnetic moments from the crystalline network are aligned (ordered) spontaneously at saturation. As a result, their magnetization is uniform and always equal to the spontaneous magnetization of the material ($M \equiv M_s$). In this case, the magnetic moment of the *single-domain nanoparticle* will be

$$m_{NP} = M_s V_{NP}, \tag{4}$$

where V_{NP} is the volume of the *single-domain* nanoparticle.

For a system of identical nanoparticles, in the absence of interactions, which has the concentration n (the number of nanoparticles (N) in the volume of the system (V_S)), each nanoparticle having the magnetic moment m_{NP} (Fig. 2), *the saturation magnetization* can be expressed by the formula

$$M_{sat,NP} = n m_{NP}, \tag{5}$$

respectively,

$$M_{sat,NP} = n V_{NP} M_s = N \frac{V_{NP}}{V_S} M_s. \tag{6}$$

This formula is also valid in the case of the system of large nanoparticles (with domain structure), but only when it is *magnetized to saturation*.

In conclusion, the magnetization of a system of nanoparticles, even if they are small or large, at *magnetic saturation* can be expressed by the formula (6), where $NV_{NP}/V_S = f_V$ represents the (volume) packing fraction of nanoparticles within the system. Therefore, the saturation magnetization of a system of nanoparticles can also be expressed by the formula

$$M_{sat,NP} = f_V M_s. \tag{7}$$

The observable f_V can take values in the range 0–1 ($0 \leq f_V \leq 1$), in the case of a system of nanoparticles. The case $f_V = 1$ corresponds to the *bulk material* (compact system), for which $M_{sat,NP} = M_s$. Equation 7 can be verified by experiment, for any given system of nanoparticles, if we take into account the value of the packing fraction of the nanoparticles.

In theory, at magnetic saturation, taking into account the magnetic packing fraction of a system of nanoparticles, there should not occur any differences between the two values $M_{sat,NP}$ and M_s; they should be equal ($M_{sat,NP} = M_s$, for $f_V = 1$). However, in practice, it has been experimentally observed that there is a difference between the two values, namely, $M_{sat,NP}$ *is smaller than* M_s ($M_{sat,NP} < M_s$) [1–9].

The difference between the saturation magnetization of a system of nanoparticles and that of the corresponding bulk material, experimentally determined, was explained by Coey, in Ref. [8] for the nanocrystallites of γ-Fe_2O_3 having the mean diameter of 5.9 nm, who showed that at the surface of small nanoparticles, the spins (magnetic moments in the crystalline network) are not ordered as they are in their inside (core), but are disposed in *disorder structure* (the surface spins are inclined at various angles). For the spin disorder at the surface of nanoparticles, several models have been proposed for different nanostructures. Coey [8] proposes the model of the inclined spins at the surface of nanoparticles, in the core–shell model: core, where the spins are normally aligned, and surface layer, where the spins are inclined to their normal direction. Berkowitz et al. [9, 10] propose for the surface spin disorder the model "spin canting," for nanoparticles of $NiFe_2O_4$, and "spin pinning" when the particles are covered with organic surfactant. Kodama and Berkowitz et al. [11] propose the model ferrimagnetically aligned core spins and a spin-glass-like surface layer, at low temperatures, where canted spins freeze in such a structure. The suface layer of nanoparticles where the spins are in a disordered structure was experimentally confirmed by Mössbauer spectroscopy for γ-Fe_2O_3 [8, 12, 13] and $NiFe_2O_4$ [14], polarized neutron scattering technique for nanoparticles of $CoFe_2O4$ [15], magnetic resonance (ESR) for the nanoparticles of $Mn_xFe_{1-x}Fe_2O_4$ ($x = 0.1 - 0.7$) with oleic acid as surfactant [16] or nanoparticles of γ-Fe_2O_3 [17] and Ni-Zn [18] dispersed in the matrix of SiO_2, as well as by transmission electron microscopy (TEM or HR-TEM) and magnetic measurements [17–20]. The surface spin disorder is due to the modification of the exchange interactions between surface magnetic ions in incomplete coordination [21].

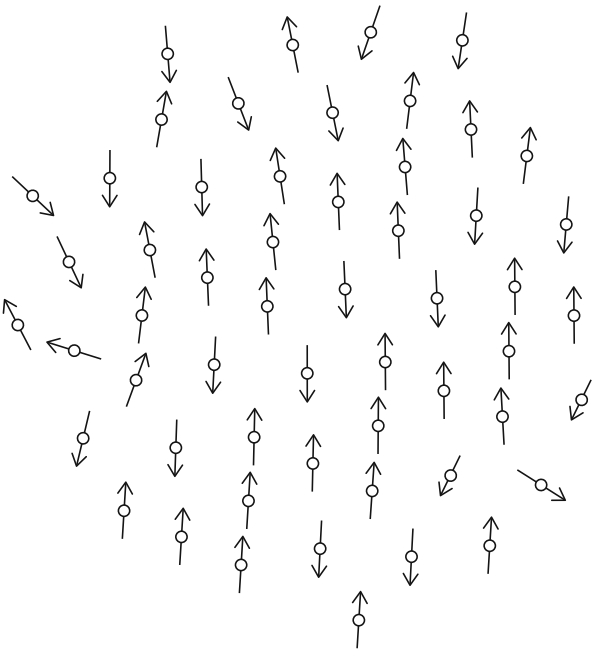

Fig. 3 Particle broken bond density $BBD = 0.8$ and higher roughness (2.1 A° RMS), hence significant surface spin disorder (Reprinted from [3], Copyright (1999), with permission from Elsevier)

In the case of ferrimagnetic nanoparticles, the orientation of the surface magnetic moments can be more altered, because the exchange interaction is done through the oxygen ion O^{2-} (*superexchange*). Therefore, the absence of the ion at the surface or the presence of another atom (ion) as impurity leads to the breaking of the exchange interaction ("broken exchange bond") between the magnetic cations, which induces the surface spin disorder [11]. Figure 3 shows the nanoparticle surface spin disorder when there is broken bond. This model was calculated for the 25 A° $NiFe_2O_4$ nanoparticle with broken bond density of 0.8 and higher roughness (with a surface anisotropy of 4 k_B/spin) [3].

The spin disorder can change the magnetic properties of nanoparticles, especially when there is a high area/volume ratio [4, 5, 22, 23]. Due to surface effects mentioned above and to the core–shell morphology, the saturation magnetization of nanoparticle systems is considerably lower than the corresponding bulk material [1–6].

Taking now into account the surface layer of the nanoparticles, *without magnetic ordering*, considering the core–shell structure (core, where the spins are aligned due to the ferro- and ferrimagnetic exchange interaction, and shell, where the spins are disposed in a disorder structure), it results that the formula (7) that gives the saturation magnetization of the nanoparticle system must take into account a volume of the nanoparticle, named *magnetic volume* ($V_{m,NP}$) (the volume of the core of the nanoparticles where the spins are aligned), smaller than the V_{NP} volume (*physical volume*),

$$V_{m,NP} < V_{NP}. \tag{8}$$

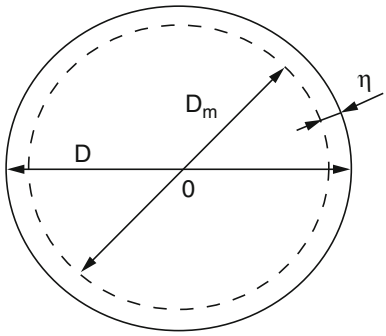

Fig. 4 Core–shell pattern of the spherical nanoparticle

In the spherical nanoparticle pattern (Fig. 4), we can assess the volume of the surface layer of the nanoparticles which contains the spins in disorder,

$$\Delta V = V_{NP} - V_{m,NP} = \pi\left(D^3 - D_m^3\right)/6, \tag{9}$$

and its thickness $\eta = (D - D_m)/2$, respectively.

Consequently, in the case of nanoparticles, the formula must be corrected, meaning that a *magnetic* (volume) packing fraction, $f_m = NV_{m,NP}/V_S$, must now be taken into account, instead of f_V, as a result of the *reduced volume* of the nanoparticles where the spins are aligned ferromagnetically. Therefore, for a system of nanoparticles, there is the relation

$$M_{sat} = f_m M_s < M_{sat,NP}, \tag{10}$$

where $f_m < 1$ ($f_m < f_V$), a formula that *corresponds to the physical reality* (verified by experimental data). The larger or smaller deviation of saturation magnetization of magnetic nanoparticles, M_{sat}, as compared to that of the bulk, M_s (or $M_{sat,NP}$ for $f_V = 1$), will depend on the existent nanostructures [2, 4, 5, 24–30].

The difference between the saturation magnetization of the bulk and that of the nanoparticles corresponding to the same material, $\Delta M_{sat} = M_{Vsat,NP} - M_{sat}$, increases as the nanoparticles are smaller. The difference decreases when the size of the nanoparticles increases, and it becomes insignificant ($\Delta M_{sat} \to 0$) at very high values of the NPs (hundreds of nm, or even more). This effect can be easily understood if the surface/volume ratio of the nanoparticles (S_{NP}/V_{NP}) is taken into account, which can be rendered, in the approximation of spherical nanoparticles:

$$S_{NP}/V_{NP} = 6/D_m. \tag{11}$$

As the magnetic volume of the nanoparticles decreases (the decrease of the diameter D_m), the ratio S_{NP}/V_{NP} will increase, reaching very high values in the nanometer domain. For example, for nanoparticles with 10 nm in diameter, the surface/volume ratio will be $S_{NP}/V_{NP} = 6 \times 10^8\,\mathrm{m}^{-1}$. For example, considering $\eta = 0.8$ nm (typical value) and assessing the contribution of the surface layer in

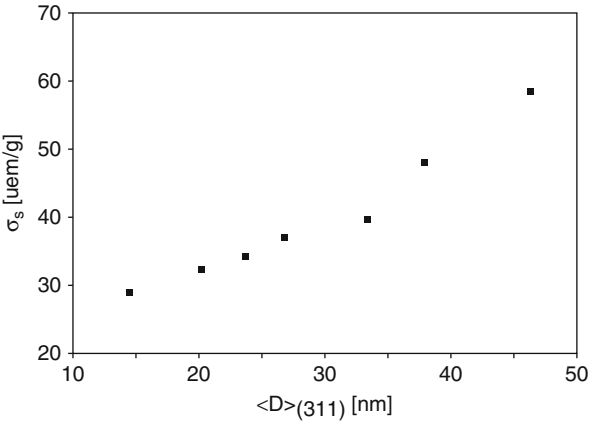

Fig. 5 Specific saturation magnetization as a function of the mean diameter of nanocrystallites [5]. © IOP Publishing (Reproduced by permission of IOP Publishing. All rights reserved)

relation to the core of the nanoparticle, $\Delta V/V_m = (V - V_m)/V_m = (D/D_m)^3 - 1$, we obtain the value 0.05 in the case of 100 nm nanoparticles and 0.69 in the case of 10 nm nanoparticle, respectively, 2.18 for 5 nm. This shows that, for small nanoparticles, the contribution of the spins from the surface of nanoparticles becomes very important and cannot be neglected, and, as a result, a significant reduction of the saturation magnetization will occur. In the case of large-sized nanoparticles, the effect is reverse; there is an increase in the contribution of the spins in the interior of nanoparticles, which will lead to an increase of the saturation magnetization, and when the contribution of the surface spins becomes insignificant, it will lead to the saturation magnetization of the bulk. Figure 5 illustrates this situation in the case of nanoparticles of Ni-Zn, when the (specific) magnetization strongly decreases when the diameter of the nanoparticles decreases [5].

Taking into account the thickness of the surface layer of NPs, we can estimate the saturation magnetization of the magnetic nanoparticle, using the formula

$$M_{sat} = M_s\left({}^{V_{m,NP}}/_{V_{NP}}\right). \tag{12}$$

Considering the NP model from Fig. 4, with the thickness of the surface layer η and the volume of the surface layer given by Eq. 9, from Eq. 12 we obtain

$$M_{sat} = M_s\frac{V_{NP} - \Delta V}{V_{NP}} = M_s\left(1 - 2\frac{\eta}{D}\right)^3 \tag{13}$$

This relation allows the estimation of the thickness of the surface layer of nanoparticles, using the experimental data: the saturation magnetization (determined by experiment) and the physical diameter D (determined, e.g., through TEM). This formula allows a more precise assessment of the thickness of the surface layer, than the one proposed in Ref. [30] ($M'_{sat} = M_s(1 - 6/D)$), which is a good approximation only for very small values of thickness, in general under 0.3 nm; at larger thicknesses, of more nm, significant errors occur when using this formula.

The situation becomes more complex in the case of surfacted nanoparticles (or covered with different molecules) or those embedded in different nonmagnetic solid matrices (crystalline or noncrystalline). After the process of preparation (through different physical and chemical methods), besides the effect discussed above, a layer at the surface of the nanoparticles can also appear as a result of different processes (adsorption, chemisorption, formation of bonds with the magnetic ions at the surface of NPs, etc.) [13, 31, 32]. The thickness of this new layer, *without magnetic ordering*, can vary from tenths of nm to 1–2 nm [18–20, 32, 33]. In these cases the issues are not yet clarified, for example, whether we can consider of two layers, as a result of the surface effect and that of the surfactant, or of a single layer determined by their cumulative effect. Many studies have been conducted on this matter [34–36], but a universally valid magnetic pattern of the nanoparticle doesn't exist. Therefore, for the practical applications in nanotechnology, it is recommended that, for each particular case, the exact values of interest be studied and determined in advance (before the application), as well as the practical values of interest, such as the saturation magnetization, the thickness of the layer from the surface of nanoparticles, surfactant or not, etc.

The Variation of the Nanoparticle Saturation Magnetization with Temperature

The *temperature variation of the saturation magnetization of nanoparticles* is a highly discussed, but not clarified issue, especially at low temperatures, and there is, currently, much research on this matter [37–43]. The surface effects (section "Surface Spin Disorder in Nanoparticles and Saturation Magnetization"), in the case of small nanoparticles, or the interface effects, in the case of surfactant or those embedded in different matrices of nanoparticles, can influence the variation of saturation magnetization with the temperature of the system of nanoparticles (see below).

At present, it becomes more clear that, at *high temperatures*, the temperature at which the saturation magnetization reaches zero (Curie temperature (T_C)), when the transition from the ferromagnetic (or ferrimagnetic) state to the paramagnetic state occurs, depends on *the size of nanoparticles*: the Curie temperature of the nanoparticle system decreases, as the diameter of nanoparticles decreases, a fact proved both experimentally and theoretically [44–49]. It was shown that the Curie temperature can be expressed in relation to diameter of nanoparticle (D) by finite-size scaling law [50] (in agreement with Monte Carlo (MC) simulation),

$$T_C(D) = T_{C,bulk}\left[1 - \left(\frac{d_0}{D}\right)^{1/\nu}\right] \tag{14}$$

where $T_{c,bulk}$ is the Curie temperature corresponding to the bulk, d_0 is a microscopic length scale close to the lattice constant [50, 51], and ν is an exponent which has the theoretical value of 0.7048 (predicted by the Heisenberg model) [52].

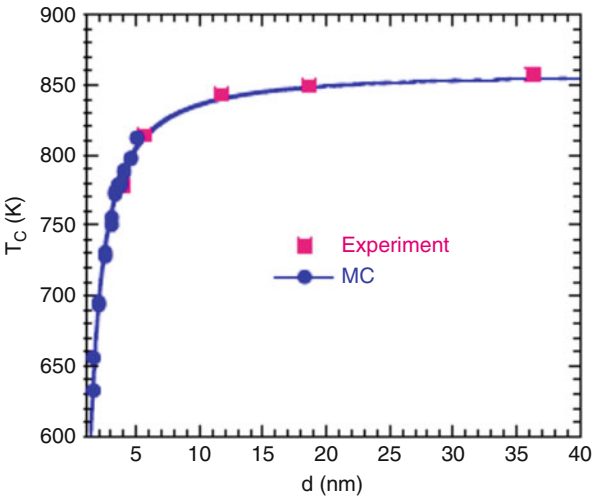

Fig. 6 (Color online) T_C's of the magnetite nanoparticles vs the mean diameter d. The solid squares are the data points obtained from experiment and solid circles represent the result obtained from MC simulations (Ref. [53]). The best fit of (14) to the MC result (*solid line*) yields $\upsilon = 0.82 \pm 0.02$ and $d_0 = 0.51 \pm 0.02$ nm (Reprinted with permission from [44], Copyright [2011], AIP Publishing LLC)

Figure 6 (where $d \equiv D$) shows such a variation in the case of Fe_3O_4 nanoparticles covered with SiO_2 [44], the experimental values being in good agreement with the ones obtained by the Monte Carlo simulation [53].

However, at *low temperatures*, the results obtained so far have shown that there is an influence of the surface layer of nanoparticles (or nanoparticle size) on the variation of saturation magnetization with temperature. We further present [40], in more detail, an interesting result, compared to literature data [3, 54–61], obtained for the variation of saturation magnetization with temperature for nanoparticles of $Mn_{0.6}Fe_{2.4}O_4$ when oleic acid surfactant was used (organic surfactant) [40, 62] and dispersed in kerosene (solvent), at a concentration $n = 4{,}58 \times 10^{22}$ m^{-3} [63] (ferrofluid sample) (With kind permission from Springer Science + Business Media: [40] © Springer-Verlag 2004). Due to the surfactant, the interactions between nanoparticles are missing, the magnetic (volume) packing fraction, $f_m = M_{sat}/M_{s,300}$ ($M_{s,300} = 448 \times 10^3$ A/m at a temperature of 300 K [55]), being only 0.031 (~3 %).

At low temperatures, the variation of the spontaneous magnetization (M_s) with the temperature (T) for the bulk is governed by the law in $T^{3/2}$ (the Bloch law) [54, 55], deduced from the spin wave model,

$$M_s(T) = \Gamma\left(1 - \Lambda T^{3/2}\right), \tag{15}$$

where Γ is the spontaneous magnetization at 0 K ($M_s(0)$) and Λ is a constant that depends on the exchange integral J ($\Lambda \sim 1/J^{3/2}$). Dependence (Eq. 15) is well verified experimentally until room temperature, both for bulk materials (Fe, Ni) [56, 57] and for some spinel ferrites (such as $Mn_xFe_{3-x}O_4$; $0{,}2 < x < 1{,}0$ [58]). Some differences can only be observed for the exponent value of temperature T (e.g., for magnetite, the exponent has the approximate value of 2).

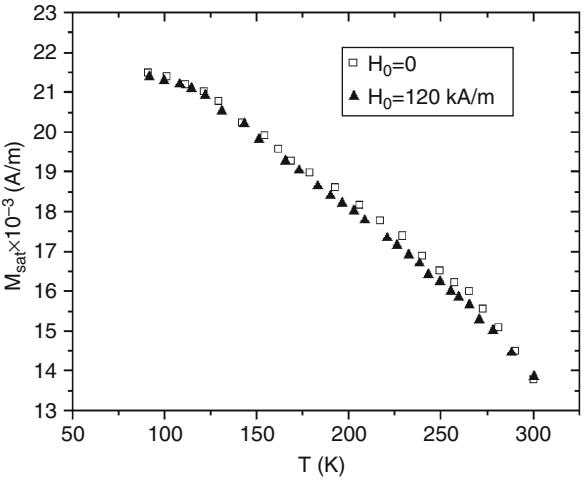

Fig. 7 Saturation magnetization as a function of temperature of the system composed of $Mn_{0.6}Fe_{2.4}O_4$ nanoparticles surfacted with oleic acid, both in the presence and in the absence of the continuous field H_0 (Springer and Applied Physics A [40], Fig. 1, © Springer-Verlag 2004. With kind permission from Springer Science and Business Media)

In the case of *fine particles* and *clusters*, some theoretical calculus and the experimental results have shown that the exponent of the temperature is higher than 3/2 [59–61]. However, Martinez et al. [3] have demonstrated experimentally that in systems made up of γ-Fe_2O_3 nanoparticles with a *diameter of* ~10–15 nm, the saturation magnetization does indeed follow the law in $T^{3/2}$ until room temperature. All these results show that the dependence, $M_s - T$, that was verified for the bulk material does not always apply to systems made up of *fine* particles and clusters, and there have been various interpretations for this behavior. Furthermore, when nanoparticles are covered with oleic acid (organic surfactant), the acid is strongly absorbed on the surface [17], and thus it forms a superficial layer [18]. This layer can influence the variation of saturation magnetization with temperature.

The variation of the saturation magnetization of the nanoparticle system in the temperature range (90–300) K is shown in Fig. 7. This was determined from the magnetization curves at saturation, which were recorded both for the sample cooled down from 300 K to 90 K, in the presence of a continuous magnetic field $H_0 =$ 120 kA/m applied along the direction where the magnetization will occur, and in the absence of this field.

Two important aspects can be observed from the diagram: (i) a rapid increase of the saturation magnetization with the decrease of temperature, with a relative variation $\Delta M_{sat}/M_{sat,300} = 55.8$ % ($\Delta M_{sat} = M_{sat,90} - M_{sat,300}$; the numeric index represents the value of the temperature) that is ~35 % higher than the relative variation of the spontaneous magnetization of bulk ferrite ($\Delta M_s/M_{s,300} \cong 21$ % [55]), in the same temperature range, and (ii) the increase of the saturation magnetization does not depend on the fact that the nanoparticles, and with their easy magnetization axes, were oriented (aligned) by the field H_0 along the subsequent measuring direction (in the absence of the field H_0, the easy magnetization axes are randomly oriented). This result shows an abnormal increase of the saturation

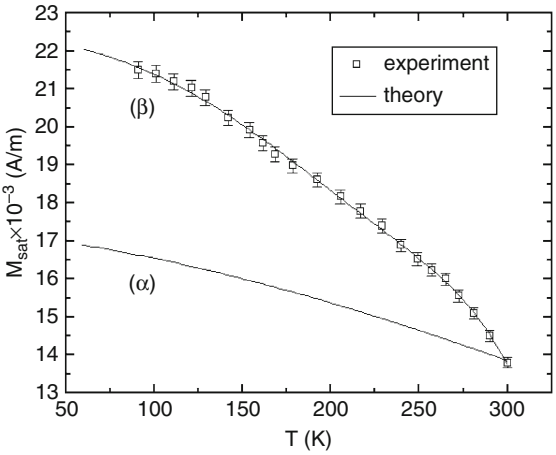

Fig. 8 Curves that represent the dependence of the saturation magnetization on temperature according to (15) (α) and (29) (β); experimental curve (□) in the absence of the continuous field ($H_0 = 0$) (Springer and Applied Physics A [40], Fig. 5, © Springer-Verlag 2004. With kind permission from Springer Science and Business Media)

magnetization of the surfacted nanoparticles, and this increase is an intrinsic property of the particle.

The dependence $M_{sat}(T)$ both for the $Mn_xFe_{3-x}O_4$ bulk ferrite ($x = 0.6$) (curve α), where $\Gamma = 17.12 \times 10^3$ A/m, $\Lambda = 3.74 \times 10^{-5}$ $K^{-3/2}$ (Eq. 15) [55], and for the sample made up of nanoparticles that are covered with oleic acid (curve □) (and which was magnetized in the absence of the continuous magnetic field) is shown in Fig. 8. The value of the constant Γ was determined based on the assumption that the saturation magnetization of the nanoparticle would follow the same variation law as bulk material (Eq. 15) and, at the same time, by taking into consideration the value of the magnetic packing fraction f_m ($\Gamma = f_m M_s(0)$, $M_s(0) = 556 \times 10^3$ A/m [64] where $M_s(0)$ is the spontaneous magnetization at 0 K. In the case of *surfacted* nanoparticles, they have found that there is a high deviation of the dependence M_{sat} vs. T from curve (α). This difference in behavior was also observed for magnetite nanoparticles covered in oleic acid [19].

This deviation is determined by the increase of the magnetic diameter attached to the nanoparticles' cores where the spins are aligned due to the superexchange interaction. This reasoning is based on their previous results [35] which have shown that the magnetic diameter of the nanoparticles *surfacted* with oleic acid increases when the temperature decreases, as it will be shown below for nanoparticles of $Mn_{0.6}Fe_{2.4}O_4$. These results led to the idea that the packing fraction f_m also increases with temperature, and this aspect *has to be* taken into consideration when determining the variation of the saturation magnetization with the temperature of the nanoparticle system.

While the saturation magnetization of bulk ferrite is the same as the spontaneous magnetization at 0 K, in the case of ferrofluids, it disappears completely since

$$M_{sat} = f_m M_s \tag{16}$$

(see section "Surface Spin Disorder in Nanoparticles and Saturation Magnetization"). Under these circumstances, the magnetic packing fraction of the nanoparticle system at a temperature T

$$f_m(T) = \frac{M_{sat}(T)}{M_s(T)} \tag{17}$$

and at 0 K,

$$f_m(0) = \frac{M_{sat}(0)}{M_s(0)}, \tag{18}$$

respectively, is not constant anymore (it increases with the decrease of temperature). Furthermore, if in the Bloch law (Eq. 15) they replace $M_s(T)$ from Eq. 17 and $M_s(0)$ from Eq. 18, we obtain the mathematical expression of the saturation magnetization of the system made up of surfacted nanoparticles

$$M_{sat}(T) = M_{sat}(0)\frac{f_m(T)}{f_m(0)}\left(1 - \Lambda \cdot T^{3/2}\right) = M_s(0)f_m(T)\left(1 - \Lambda \cdot T^{3/2}\right). \tag{19}$$

In a more restricted form, the temperature dependence of the saturation magnetization of the surfacted nanoparticle system is

$$M_{sat}(T) = \Gamma(T)\left(1 - \Lambda T^{3/2}\right), \tag{20}$$

where the parameter

$$\Gamma(T) = M_s(0)f_m(T) \tag{21}$$

is a *function of temperature* and not a *constant*, as in the case of bulk ferrite.

Provided f_m did not depend on temperature and were a *constant* (the same as the one at room temperature), Eq. 19 would be reduced to the Bloch law for bulk material (Eq. 15), where $\Gamma \equiv M_s(0) = const.$, and the increase of the saturation magnetization of the system would be a result of the variation of the spontaneous magnetization with temperature.

When f_m *is no longer a constant* and *it depends on temperature* (as in their case), a further term has to be included in the equation to reflect this aspect (i.e., the increase of the nanoparticle magnetic moment and of the magnetic diameter, with the decrease of temperature); in other words, the law has to be considered as it was written in Eq. 19.

Because the saturation magnetization of the nanoparticle system is

$$M_{sat}(T) = nm_{m,NP}(T) = nV_m(T)M_s(T) \tag{22}$$

in agreement with Eq. 17, it results that

$$f_m(T) = n\pi \langle D_m(T) \rangle^3 / 6 \tag{23}$$

(in the approximation of spherical nanoparticles). By replacing $f_m(T)$ in Eq. 19, we obtain

$$M_{sat}(T) = M_s(0)(n\pi/6)\langle D_m(T)\rangle^3 \left(1 - \Lambda \cdot T^{3/2}\right). \tag{24}$$

In Eq. 24, $\langle D_{\mathrm{m}}(T) \rangle$ is the mean magnetic diameter of the nanoparticles as a *function of temperature*. In agreement with Eq. 24, it can be concluded that the considerable increase of the saturation magnetization of a system made up of surfacted nanoparticles, compared to that of bulk ferrite, is a result of the increase of the mean magnetic diameter $\langle D_{\mathrm{m}} \rangle$ of the nanoparticles (in which the spins are aligned by means of the superexchange interaction), because $n \cong const.$ and the increase of the spontaneous magnetization $M_s(T)$ when the temperature decreases from 300 to 77 K (Fig. 8, curve α) is much lower. Our explanation for this behavior is attributed to the modification of the superexchange energy (W_{sch}) in the surface layer of the nanoparticles due to the presence of surfactant molecules [35]. Consequently, the Néel temperature ($T_N \cong W_{sch}/k_B$, k_{B} – Boltzmann constant) in the superficial layer will change, and it will be lower than the room temperature. As the temperature decreases, T_{N} of the sublayers that are adjacent to the magnetic core of the nanoparticles will be exceeded gradually, so that these sublayers will successively become ferrimagnetically ordered. The result is an increase of the magnetic diameter $\langle D_{\mathrm{m}} \rangle$ attached to the core where the spins are aligned, with the decrease of temperature; this will in turn lead to an increase of the magnetic packing fraction f_{m} and, implicitly, of the saturation magnetization for the nanoparticle system.

In a different approach, from Eq. 22 at temperature T ($T < 300$ K) and at room temperature, they obtain

$$\langle D_m(T)\rangle^3 = \langle D_m\rangle_{300}^3 \left(\frac{M_s}{M_{sat}}\right)_{300} \frac{M_{sat}(T)}{M_s(T)}. \tag{25}$$

The mean magnetic diameter $\langle D_{\mathrm{m}} \rangle_{300}$ at a temperature of 300 K was determined from the magnetization curve, with the procedure described in Ref. [34], admitting a lognormal distribution of the magnetic diameters and the dependence of the particle's magnetic moment on the diameter. This way, we have found $\langle D_{\mathrm{m}} \rangle_{300} =$ 10.8 nm. Considering that in the case of the nanoparticles surfacted with oleic acid at their surface, a superficial layer is formed and its mean thickness is 0.7 nm [32, 65–67],

$$\langle \eta \rangle_{300} = \left(\langle D \rangle - \langle D_m \rangle_{300}\right)/2 = 0.7\,\mathrm{nm}, \tag{26}$$

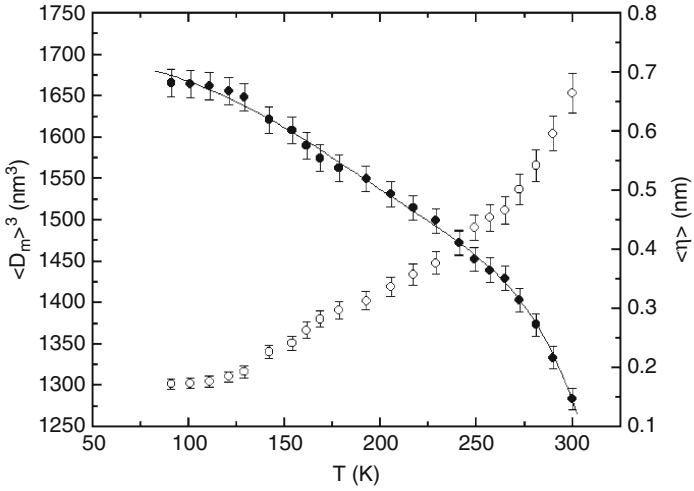

Fig. 9 $\langle D_{\mathrm{m}}(T)\rangle^3$ vs T (•) and $\langle\eta\rangle$ vs T (○) of the nanoparticles; (—) fit curve of $\langle D_{\mathrm{m}}(T)\rangle^3$ (Springer and Applied Physics A [40], Fig. 6, © Springer-Verlag 2004. With kind permission from Springer Science and Business Media)

the mean physical diameter of the nanoparticles is also obtained:

$$\langle D\rangle = 12.2\,\mathrm{nm}. \tag{27}$$

Replacing in Eq. 25 the values $M_{\mathrm{sat}}(T)$ (Fig. 8, (□)), $M_{\mathrm{s}}(T)$ (Fig. 8, curve (α)), and $\langle D_{\mathrm{m}}\rangle_{300}$, we have calculated $\langle D_m(T)\rangle^3$. The resulting values are shown in Fig. 9.

According to Eq. 26, given that the magnetic diameter increases, the surface layer is narrowing when the temperature decreases (Fig. 9, curve ○). A proof for the fact that the determined values of the diameters $\langle D\rangle$ and $\langle D_{\mathrm{m}}\rangle$ are correct is that at the lowest temperature (90 K), the diameter $\langle D_{\mathrm{m}}\rangle_{90} = 11.9$ nm does not exceed the physical diameter $\langle D\rangle$ (12.2 nm). These results make them admit that the layer on the surface of the nanoparticles is paramagnetic at 300 K. As the temperature decreases, the layer gradually becomes magnetically ordered, starting from the core and towards the shell. Using the electron spin resonance technique, Upadhyay et al. [68, 69] have recently shown the existence of the paramagnetic shell of the $Mn_xFe_{1-x}Fe_2O_4$ ($x = 0.1$–0.7) nanoparticles in ferrofluid, surfacted with oleic acid. The authors have highlighted the existence of two absorption lines in the ESR spectrum: one that appears due to the ferrimagnetic core and another one that corresponds to $\varepsilon = 4$ (ε – the spectroscopic splitting factor), attributed to the Fe^{3+} ion in the complex structure made up of oleic acid molecules. The line with $\varepsilon = 4$ disappears at low temperatures. Similarly, Tronc et al. [70] have used Mössbauer spectroscopy at low temperatures to highlight the existence of the paramagnetic layer on the surface of *phosphated* γ-Fe_2O_3 nanoparticles.

The variation shape of the function $\langle D_m(T)\rangle^3$ in Eq. 24 was determined by fitting the experimental values (Fig. 9(•)). The variation can be approximated very well with the function

$$\langle D_m(T)\rangle^3 = \sum_{q=0}^{4} c_q T^{2q} \tag{28}$$

(c_q are known constants that were determined from the fit). A good resemblance of the fit curve and the experimental curve can also be obtained if there are two fitting coefficients; however, in order to obtain a more realistic variation of the magnetic diameter with the temperature, they have also considered the higher-order terms of T^2. The same variation form of $< D_m >^3$ with temperature was observed for Fe_3O_4 nanoparticles with a diameter of ~11 nm, covered in oleic acid and dispersed in kerosene [71]; however, the fitting coefficients (especially the first two) are different, since they depend on the nature of the material.

Under these circumstances, Eq. 24 can be written as

$$M_{sat}(T) = M_s(0)\frac{n\pi}{6}\left(\sum_{q=0}^{4} c_q T^{2q}\right)\left(1 - \Lambda T^{3/2}\right). \tag{29}$$

By building the function $M_{sat} - T$ defined by Eq. 29, with the known values of $M_s(0)$ (556×10^3 A/m), n (4.58×10^{22} m^{-3}), Λ (3.74×10^{-5} $K^{-3/2}$), and c_q (constants) that resulted from the fit, we have obtained curve (β) in Fig. 8. It can be observed that there is a very good agreement of the calculated curve (—) with the experimental curve (□), which demonstrates that function Eq. 29 is suited to describe the temperature variation of the saturation magnetization of the system composed of surfacted nanoparticles. The result obtained justifies the correctness of the function Eq. 29 that we have suggested for describing the variation of the saturation magnetization of the surfacted nanoparticle system with the temperature in a range of low temperatures.

Magnetic Anisotropy of Nanoparticles

The issue of the magnetic anisotropy of nanoparticles is very important, because it has a significant influence on their magnetic behavior in an exterior magnetic field. In the case of nanoparticles, there are several components of the magnetic anisotropy, which must be considered in the total energy of a crystal, when making a thorough magnetic (micromagnetic) analysis. These are the magnetocrystalline anisotropy (W_V), the anisotropy due to the shape (W_{sh}), surface anisotropy (W_s), and an induced anisotropy (of different effects) (W_i). Therefore, the total energy of a crystal in an external magnetic field (H) will be written as

$$W = W_{ex} + W_m + W_H + W_w + W_a \tag{30}$$

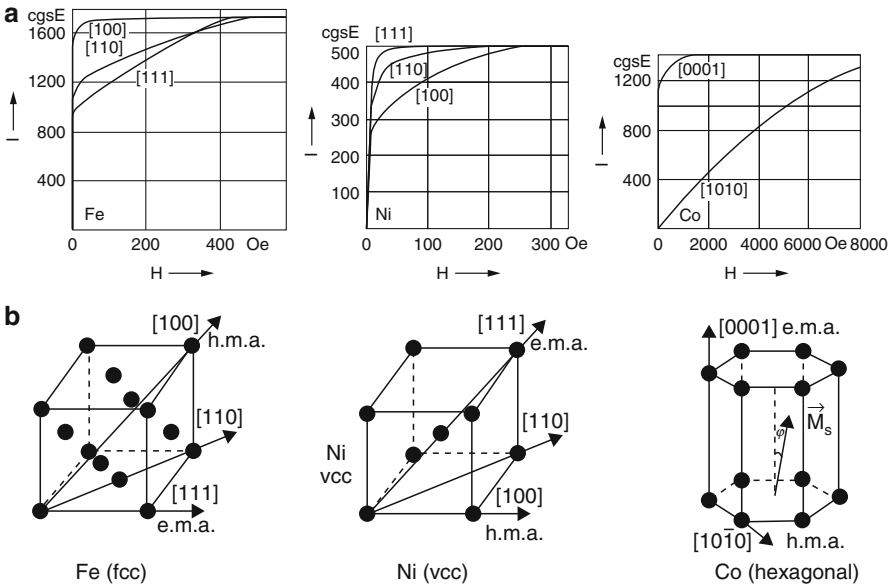

Fig. 10 (**a**) Magnetization curves of Fe-, Ni-, and Co-single crystal depending on the fundamental directions (Springer [75], Fig. 13.1, © Springer-Verlag 1962. With kind permission from Springer Science and Business Media). (**b**) The crystallographic systems for Fe-, Ni-, and Co-single crystal

where W_{ex} is the exchange energy, W_m is the magnetostatic energy, W_H is the energy in the external magnetic field, W_w is the energy of the magnetic domain wall (when it exists (for large nanoparticles)), and W_a is the anisotropy energy,

$$W_a = W_V + W_{sh} + W_s + W_i. \tag{31}$$

They present below each of the four types of magnetic anisotropy that may exist in the case of nanoparticles.

Magnetocrystalline anisotropy. In the case of nanoparticles, as in the case of the bulk, macroscopically, the magnetization of a single crystal in an external magnetic field depends on the direction in which this occurs in relation to its crystallographic axes (Fig. 10a). This leads to the existence of a *magnetocrystalline anisotropy*. The direction in the crystal in which the magnetization occurs the easiest (the mechanical work of the magnetization, $\mu_0 \int HdM$, is the lowest) is the *easy magnetization axis* (e.m.a.), and the direction in which the magnetization occurs the hardest (the mechanical work of the magnetization is the highest) is the *hard magnetization axis* (h.m.a.). For example, for Fe, the directions |100|, |010|, and |001| (the edges of the cube) are easy magnetization axes, and the direction |111| (large diagonal of the cube) is the hard magnetization axis [72]. The first magnetization curves of single crystals of Fe [72], Ni [73], and Co [74] depending on the directions of

magnetization (in Kneller [75]) and their crystallographic systems with easy and hard magnetization axes are shown in Fig. 10a.

In order to rotate the spontaneous magnetization vector from the direction e.m.a. in a different direction, set by direction cosines α_1, α_2, and α_3 in relation to the crystallographic axes, mechanical work of magnetization is needed, the variation of which is equal to the *magnetocrystalline anisotropy energy*. In the phenomenological model based on the symmetry properties of the crystal [76, 77], the magnetocrystalline anisotropy energy can be expressed by a power series formula, which in the case of *cubic symmetry* (Fe, Ni) has the expression

$$W_{V,c} = K_1\left(\alpha_1^2\alpha_2^2 + \alpha_1^2\alpha_3^2 + \alpha_2^2\alpha_3^2\right) + K_2\alpha_1^2\alpha_2^2\alpha_3^2 + K_3\left(\alpha_1^4\alpha_2^4 + \alpha_1^4\alpha_3^4 + \alpha_2^4\alpha_3^4\right) + \ldots, \quad (32)$$

where K_1, K_2, K_3 are the *magnetocrystalline anisotropy constants* (energy densities). In the formula (32), in agreement with the experiment data, they can most often consider only the first two terms of the series, the third term being insignificant, since it is usually very small.

In the case of *hexagonal symmetry* (*uniaxial*) (Co), the magnetocrystalline anisotropy energy is given by the relation [78]

$$W_{V,u} = K_{1u}\sin^2\varphi + K_{2u}\sin^4\varphi + \ldots, \quad (33)$$

where φ is the angle between the spontaneous magnetization vector and the main axis of symmetry (see Fig. 10c). Developments regarding the magnetocrystalline anisotropy, which better reflect the symmetry properties of the crystal, were made by Kneller and van Vleck [79].

Anisotropy energy can also be expressed in relation to the *anisotropy field* (H_V), through the relation

$$W_V = -\mu_0\left(\vec{M}_s \cdot \vec{H}_k\right). \quad (34)$$

In the case of uniaxial symmetry, in the approximation $K_{2u} << K_{1u}$, it can be written as

$$H_{V,u} = \frac{2K_{1u}}{\mu_0 M_s}. \quad (35)$$

Usually, when only the anisotropy constant K_1 is used in the formulas of anisotropy (field) energy, it is simply written as K instead of K_1, without using indices (e.g., $H_{V,u} = 2K_u/\mu_0 M_s$).

Shape magnetic anisotropy. Since nanoparticles can have different shapes, their magnetization will also depend on the shape.

In the case of a single crystal of ellipsoidal shape (ellipsoid of revolution) with the ellipsoid axes $a >> b = c$ (Fig. 11), the anisotropy energy due to shape is [75]

$$W_{sh} = (\mu_0/2)(N_a - N_b)M_s^2\sin^2\theta \quad (36)$$

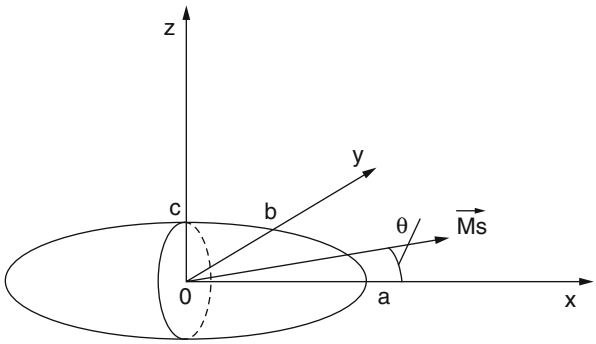

Fig. 11 Single crystal of ellipsoidal shape; θ is the angle between spontaneous magnetization vector $\vec{M}_s$ and the axis 0a of the ellipsoid

where N_a and N_b are *demagnetization factors* of the axes a and b, respectively, of the ellipsoid and θ is the angle that the spontaneous magnetization makes with the major (a) axis of the ellipsoid. Considering Eq. 33, in the first-order approximation, the anisotropy constant due to shape can be expressed by the formula

$$K_{sh} = -\mu_0(N_b - N_a)M_s^2/2. \tag{37}$$

In the case of *spherical nanoparticle*, since $N_a = N_b$ and, therefore, $K_{sh} = 0$, there is no shape anisotropy. However, in the case of elongated and soft magnetic nanoparticles, such as some ferrites (ferrimagnetic nanoparticles), the shape anisotropy constant can become comparable to or even higher than the magnetocrystalline anisotropy constant [19].

Surface magnetic anisotropy. The problem of surface anisotropy was studied in detail by Neel [80, 81], which showed that in the case of crystals with cubic symmetry and surfaces of the type |111| and |100|, the surface anisotropy energy can be expressed by the formula

$$W_s = K_s \cos^2\beta, \tag{38}$$

where K_s is the *surface anisotropy constant* (expressed in Jm^{-2} in IS) and β is the angle between the spontaneous magnetization vector and the direction of the external normal at the surface considered. Expressing the surface anisotropy energy constant in units Jm^{-3} [82, 83], considering relation (11),

$$K_s'\left[\mathrm{Jm}^{-3}\right]_{IS} = (6/D)K_s\left[\mathrm{Jm}^{-2}\right]_{IS}, \tag{39}$$

and comparing it with the magnetocrystalline anisotropy constant, it is found that the value of K'_s becomes significant for nanoparticles. Moreover, when the diameter of the nanoparticles is low enough, generally less than 25 nm in many cases of soft magnetic materials, the value of the surface anisotropy constant exceeds the magnetocrystalline anisotropy constant, being the greater as the nanoparticle diameter is smaller. For example [84], in the case of nanoparticles of Ni-Zn ferrite with a diameter of 10 nm, considering the value of the constant K_s which is of the order of

10^{-5} Jm^{-2} [85], the value obtained for K'_s is 6×10^3 Jm^{-3}. This value is five times higher than the magnetocrystalline anisotropy constant ($1{,}5 \times 10^3$ Jm^{-3} [86]) of Ni-Zn ferrite. In conclusion, in the case of small nanoparticles, the contribution of the spins at the surface layer of nanoparticles to the magnetic anisotropy becomes important, sometimes even dominant.

Induced magnetic anisotropy. In the case of nanoparticles, as a result of mechanical, radiation processes, heat treatments, etc., or of their methods of preparation, that can lead to the presence of *elastic tension*s in the material or to the *existence of magnetic coupling between spins* (e.g., to the nanoparticle - matrix interface or of two different magnetic materials (ferromagnetic core–shell paramagnetic)), a magnetic anisotropy can be *induced*, because the equilibrium position of the spontaneous magnetization vector can be influenced. The results of the experiments showed that the elastic tensions can induce very large magnetic anisotropy, with one to two orders of magnitude larger than the magnetocrystalline. For example [84], in the case of γ-Fe_2O_3 nanoparticles, Vassiliou et al. [87] obtain the anisotropy constant value of 4.4×10^5 J/m^3 for 8.3 nm diameter nanoparticles embedded in polymer matrix, and Coey et al. [88] obtain the value of 1.2×10^5 J/m^3 for nanoparticles of 6.5 nm. These values are about two orders of magnitude higher than the magnetocrystalline anisotropy constant of *bulk* ferrite of γ-Fe_2O_3, which is $K_V = 4.6 \times 10^3$ J/m^3 [89, 90]. The pronounced effect obtained was attributed to the elastic tensions (stress) exerted on nanoparticles by the solid polymer matrix in which these can be found. Another cause of the increase of magnetic anisotropy is the presence of an antiferromagnetic or paramagnetic layer at the surface of nanoparticles (core–shell structure), due to the exchange coupling between core and shell [91].

Taking into account all the four forms of magnetic anisotropy that can exist in the case of nanoparticles and their cumulative contribution to the total magnetic anisotropy, they may consider an *effective* (total) magnetic anisotropy energy, that is, an *effective* magnetic anisotropy constant [18],

$$K_{eff} = K_V + K_{sh} + K'_s + K_i, \tag{40}$$

where K_i is the constant of anisotropy resulted from the *induced* magnetic anisotropy.

The rigorous study (theoretical) of the magnetic anisotropy for nanoparticles can be done by considering the nanoparticle as a *system of spins* $\left(\vec{S}_i\right)$ [92–97], taking into account all the magnetic interactions possible, where in Eqs. (30) and (31) the energies are given by the Dirac-Heisenberg Hamiltonian (tridimensional (0xyz)). For example, taking into account only the exchange interaction and the interaction with the external magnetic field, and considering a magnetocrystalline anisotropy (cubic) for the core of nanoparticle and a surface anisotropy for the surface spins, the Hamiltonian of the system of spins will be

$$\mathcal{H} = \mathcal{H}_{ex} + \mathcal{H}_H + \mathcal{H}_V + \mathcal{H}_s \tag{41}$$

and [97]

$$\begin{aligned}\mathcal{H} = & -2\sum_{(i\neq j)} J_{ij}\left(\vec{S}_i \cdot \vec{S}_j\right) \\ & - g\mu_B \vec{H} \cdot \sum_i \vec{S}_i - K_V \sum_i \left(S_{x,i}^2 S_{y,i}^2 + S_{y,i}^2 S_{z,i}^2 + S_{x,i}^2 S_{z,i}^2\right) \\ & - K_s \sum_k \left(\vec{S}_k \cdot \vec{e}_k\right)^2, \end{aligned} \tag{42}$$

respectively, where g is the Landé factor, μ_B is the Bohr magneton, and $\vec{e}$ is the unit vector normal on the surface.

Magnetic Behavior of Nanoparticles in an External Magnetic Field

It is very important to know, from both a practical and a theoretical point of view, how a nanoparticle magnetic system behaves when it is magnetized in an external magnetic field. It was found that the magnetic behavior of nanoparticles is much different from that of the corresponding bulk material, as it is strongly influenced by the *size of the nanoparticles*, which determines a specific behavior. These issues are presented below, starting from larger nanoparticles, which have a multi-domain or single-domain magnetic structure, until reaching nanoparticles without magnetic domains but with fluctuating magnetization (superparamagnetic).

Hysteresis Magnetic Behavior of Nanoparticles

Hysteresis Magnetic Behavior of Multi-domain Nanoparticles

Large nanoparticles, which have a size above a certain critical value (D_c) (see section "Introduction"), have a magnetic domain structure, and their behavior when magnetized (static) in an exterior magnetic field is with *hysteresis*, similarly to the corresponding *bulk* magnetic material [75, 98]. Stable magnetic structures depend on the crystal symmetry (Fig. 12), the most common experimentally observed

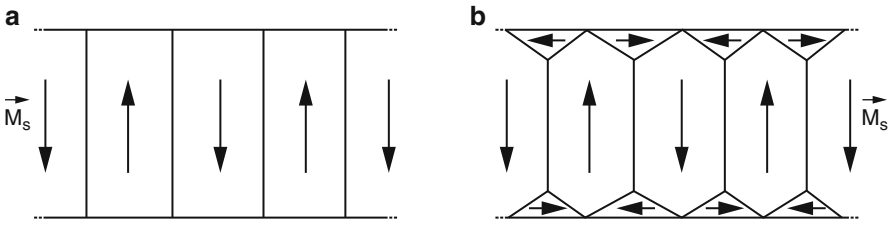

Fig. 12 Magnetic domain structures in large nanoparticles; (**a**) the uniaxial and (**b**) cubic symmetry

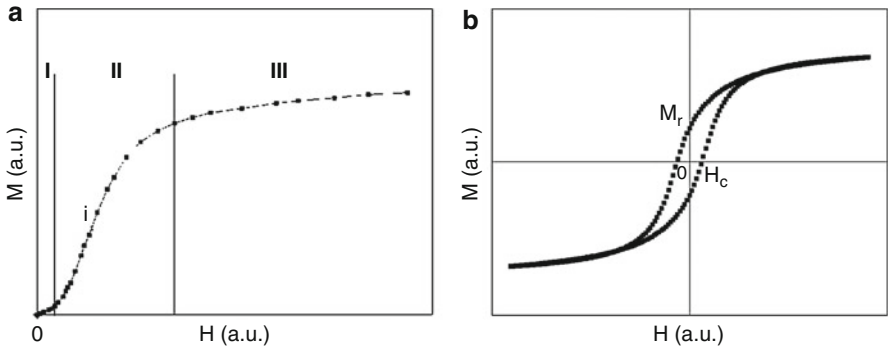

Fig. 13 First magnetization curve (**a**) and the hysteresis loop (**b**) characteristic of nanoparticles with magnetic domain structure

structures being those with free magnetic poles, in the case of uniaxial symmetry (Fig. 12a), or without free magnetic poles (with magnetic flux closure domains) (Fig. 12b), in the case of cubic symmetry. In closing domains (Fig. 12b), the spontaneous magnetization is oriented at an angle of 45° in relation to the surface of the wall of the closing domain, so no additional magnetostatic energy appears. The number of magnetic domains in a stable structure can be determined from the minimization condition of the crystal energy (equilibrium condition).

The magnetization of nanoparticles with domain structure takes place through processes of magnetic domain wall displacement, reversible and irreversible, in smaller fields and through rotation processes of the spontaneous magnetization vector, reversible and irreversible, in large fields, when the walls are missing (the structure becoming single domain).

The magnetization curve (the first magnetization) is, in this case, the typically known, generally characteristic to a ferromagnetic (or ferrimagnetic) bulk material (Fig. 13a): the incipient part (I), approximately linear (at low fields); the part of the transition from moderate fields (II), with point of inflection (i); and the part to magnetic saturation (III), from the high fields.

At low fields (up to approx. $H_c/10$ (H_c is the coercive field)), Rayleigh's law applies, which gives the variation of magnetization when applying a variation of the external magnetic field ΔH,

$$\Delta M = \chi_i \Delta H + \frac{\alpha}{2}(\Delta H)^2 \tag{43}$$

where χ_i is the initial magnetic susceptibility and α a coefficient.

At high fields, the magnetization is well described by the law of approach to saturation (LAS) [99]

$$M = M_s\left(1 - \frac{a}{H} - \frac{b}{H^2} - \frac{c}{H^3} \cdot \cdot \cdot\right) + \chi_0 H, \tag{44}$$

where a, b, and c are some coefficients and the term $\chi_0 H$ is determined by the presence of the contribution χ_0 (para-process), independent of the field. The term $\chi_0 H$ becomes more significant when the sample approaches the Curie temperature. However, experimental measurements [99, 100] indicated that, in the case of the nanoparticles, a relation of the following form is often sufficient [3, 100, 101]:

$$M \cong M_s\left(1 - \frac{b}{H^2}\right), \tag{45}$$

since the $\chi_0 H$ terms and the one in H^{-3} can be neglected and the presence of the term in H^{-1} is not justified, except in certain cases (its presence would imply an infinite magnetization which cannot be the result of rotation of the magnetization processes). The coefficient b from the formula (45) depends on the magnetic anisotropy. In the case of *uniaxial* symmetry, it has the expression [102]

$$b = \frac{4}{15}\left(\frac{K_u}{\mu_0 M_s}\right)^2, \tag{46}$$

and in the case of *cubic* symmetry [99],

$$b = \frac{8}{105}\left(\frac{K_1}{\mu_0 M_s}\right)^2. \tag{47}$$

For a system of magnetic nanoparticles, relations (46) and (47) allow the *determination of the magnetic anisotropy constants* by means of experiment (from the saturation magnetization curves), which is commonly used in current practice [3, 101].

In the transition area, at moderate fields, a law that correctly describes the magnetization of the nanosystem doesn't exist, the magnetization curves obtained experimentally being characteristic of each type of material.

At the magnetization–remagnetization of nanoparticles, a hysteresis loop is obtained (Fig. 13b) with the value of the saturation magnetization (M_{sat}) dependent on the surface effects (see section "Surface Spin Disorder in Nanoparticles and Saturation Magnetization") and the coercive field (H_c) strongly dependent on the size of nanoparticles (see section "Single-Domain Nanoparticles in the Area of Sizes Where Fluctuations in Magnetization Exist: The Coercive Field of Nanoparticles"). The curves in Fig. 13 are given for a γ-Fe_2O_3 nanoparticle system with a mean diameter of ~35 nm, which have the structure of the magnetic domains. Nanoparticles were obtained by using the method described in Ref. [5].

The *critical volume*, that is, the *critical diameter* for spherical nanoparticles corresponding to the transition from a *structure with magnetic domains* (multi-domains), with *nonuniform* magnetization, to a *single-domain structure*, with *uniform* and *stable* magnetization, can be determined from the condition of minimization of the energy of the crystal (equilibrium condition) using the single-domain particle model [103]. Reducing the volume of a large nanoparticle

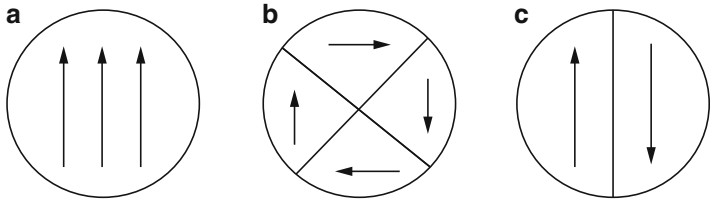

Fig. 14 Magnetic structures in spherical nanoparticle model; (**a**) uniform magnetization; nonuniform magnetization in the case of (**b**) cubic and (**c**) uniaxial symmetry (© Eurobit 2004. Reprinted with permission from Ref. [84])

(tens of nm), which has a magnetic domain structure, a certain critical size can be reached in which the nanoparticle does not have a domain structure anymore, consisting of a magnetic single domain with uniform magnetization (*single-domain structure*). Kittel [103] is the first to point out that certain geometries can lead to a uniform magnetization, thus without magnetic domains. The problem that arises in this case is at which size a structure without magnetic domains (single domain) is obtained, so that the energy of the single-domain configuration is lower than that corresponding to a nanoparticle that has a structure of domains. The answer to this problem can be obtained based on the condition that the free energy of a nanoparticle with uniform magnetization is equal, to the limit, to the free energy of a nanoparticle that has a domain structure (the classical model of the single-domain particle) [103–105]. We consider below two cases of domain structures [84, 106] (With permission from Eurobit: [84]).

(*I*) *The case of cubic symmetry*. For the single-domain structure (Fig. 14a), the energy is determined only by the magnetostatic energy:

$$W_1 = W_m = \frac{1}{2}\mu_0 N M_s^2 V, \tag{48}$$

where N is the demagnetizing factor ($N = 1/3$ for spherical particles). In the case of structure with cubic symmetry, shown in Fig. 14b, the main contribution to the energy is given by Bloch walls. Thus, we can write

$$W_2 = 2W_w = 2\varepsilon_w S \tag{49}$$

where S is the surface of a wall. Expressing the volume and the surface of the nanoparticle, considered as spherical, according to the diameter, and equalizing to the limit the two energies,

$$W_1 = W_2, \tag{50}$$

we obtain the relation

$$D_c = \frac{18\varepsilon_P}{\mu_0 M_s^2}, \tag{51}$$

which gives the *critical diameter* (or *critical volume*, $V_c = \pi D_c^3/6$). In agreement with this result, when the nanoparticle has a smaller diameter than the critical diameter ($D < D_c$), the nanoparticle is single domain and has uniform magnetization. On the contrary, when the diameter of the nanoparticle is greater than the critical diameter ($D > D_c$), the nanoparticle has a magnetic domain structure, its magnetization being nonuniform.

(*II*) *The case of uniaxial symmetry*. Considering for this case, the structure of domains from Fig. 14c at the nanoparticle's energy will contribute, on the one hand, the magnetostatic energy (structure without closing poles) and, on the other hand, the energy of the existing domain wall. Due to the presence of the two domains (magnetized at 180°), the magnetostatic energy will be reduced to half, as compared to the cases where there is a single domain (Fig. 14a). Thus, in this case, the energy of the structure can be written as

$$W_2' = \frac{W_m}{2} + W_P. \tag{52}$$

Imposing now the condition given by the rel. (50), where instead of W_2 they use W'_2 given by relation (52), it results

$$W_m = \frac{W_m}{2} + \varepsilon_P S. \tag{53}$$

Replacing the magnetostatic energy (Eq. 48), we obtain the critical diameter for uniaxial symmetry,

$$D_c = \frac{18\varepsilon_P}{\mu_0 M_s^2}, \tag{54}$$

below which the nanoparticle has a single-domain structure with uniform magnetization. By comparing Eqs. 51 and 54, they observe that, regardless of the model chosen for the domain structure (with cubic symmetry (b) or uniaxial (c)), the formula for the critical diameter remains the same.

The energy density of the domain wall ε_p was determined by Landau-Lifshitz [107] based on the exchange energy and the anisotropy of the wall involved in the spin orientation. For this, the following formula was found:

$$\varepsilon_p = \sqrt{\frac{2k_B T_c K_V}{a}}, \tag{55}$$

where "a" is the lattice constant and k_B is Boltzmann's constant.

Calculations made for Fe led to a critical diameter of ~34 nm and for Co of ~60 nm [84], the values mostly depending on the existent of the magnetic anisotropy. In the case of soft ferrites, the critical diameter decreases considerably, reaching values of ~15 nm. For example, for the $Ni_{0,35}Zn_{0,65}Fe_2O_4$ ferrite nanoparticles, we found $\varepsilon_p = 0.145$ erg/cm^2 and $D_c = 21.6$ nm [106]. In the case

of hard ferrites, e.g., the Co ferrite nanoparticles, the calculations made lead to the value of 162 nm for a critical diameter [101].

They must mention here that, in specific cases, in agreement with the issues presented in sections "Saturation Magnetization of Nanoparticles" and "Magnetic Anisotropy of Nanoparticles," they must consider both the size and the type of nanoparticles, so that the observables M_{sat}, K_{eff}, and T_C are corrected. In this respect, they must consider their experimentally determined values, knowing that M_{sat}, K_{eff}, and T_C, in the case of nanoparticles, have different values from those of the bulk material. By not taking these aspects into account, the results can lead to significant errors.

Hysteresis Magnetic Behavior of Single-Domain Nanoparticles

Single-Domain Nanoparticles with Stable Magnetization

As shown in the previous paragraph, nanoparticles that have a smaller volume than the *critical volume* ($V < V_c$) have a single-domain structure with uniform and stable magnetization. Their magnetization in an external field will be made by *rotation processes* (reversible and irreversible) of the spontaneous magnetization vector. The magnetic behavior of a single-domain nanoparticle system with stable magnetization [84] can be achieved using the Stoner-Wohlfarth (S-W) model [108] (et al. [109, 110]). Thus, considering an isolated single-domain nanoparticle with uniaxial anisotropy, in the absence of thermal agitation ($T = 0$) (or if this is low enough so it cannot reverse the magnetization of the nanoparticle), in the external magnetizing field H, the density of the energy of the particle is

$$w = K_u \sin^2\varphi - \mu_0\left(\vec{M}_s \cdot \vec{H}\right). \tag{56}$$

They consider the x0y plan, so that the 0x axis coincides with the direction of easy magnetization of the nanoparticle and the 0y axis with the hard magnetization direction (perpendicular to the 0x axis) (Fig. 15).

Expressing the vectors $\vec{H}$ and $\vec{M}_s$ according to their components on the two directions,

$$\vec{H} = H_x\ \vec{i}\ + H_y\vec{j} \tag{57}$$

and

$$\vec{M}_s = M_x\ \vec{i}\ + M_y\ \vec{j} = (M_s\cos\varphi)\ \vec{i}\ + (M_s\sin\varphi)\ \vec{j}\ , \tag{58}$$

the energy from Eq. 56 will be given by the formula (in Kneller [75])

$$w = K_u \sin^2\varphi - \mu_0 H_x M_s\cos\varphi - \mu_0 H_y M_s \sin\varphi. \tag{59}$$

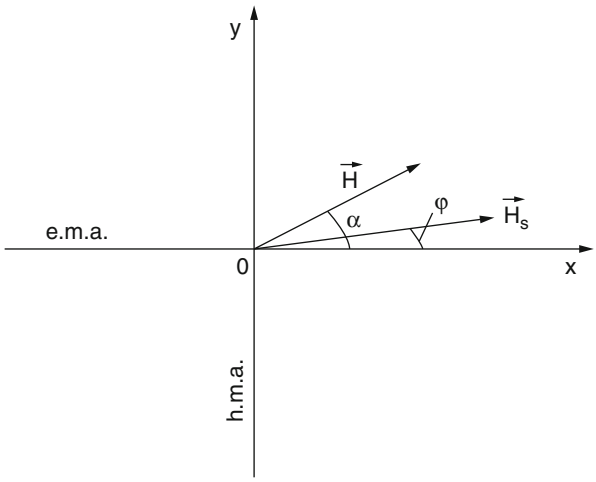

Fig. 15 The orientation of the vectors of spontaneous magnetization and magnetic field in the plan x0y

In Eq. 59 α is the angle between the external magnetic field $\vec{H}$ and the easy magnetization axis, and φ is the angle between the spontaneous magnetization $\vec{M}_s$ and the same axis (e.m.a.) (Fig. 15).

The equilibrium magnetization is obtained from the condition of minimum energy

$$\frac{dw}{d\varphi} = 0. \tag{60}$$

Thus, they obtain

$$h_x \sin\varphi - h_y \cos\varphi = -\frac{1}{2}\sin(2\varphi), \tag{61}$$

which is a straight line in the plan ($h_x 0 h_y$) for $\varphi = const.$. In Eq. 61 they considered the reduced fields, $h_x = H_x/H_{V,u}$ and $h_y = H_y/H_{V,u}$, where $H_{V,u} = 2K_u/(\mu_0 M_s)$ is the uniaxial anisotropy field and K_u is the uniaxial anisotropy constant of the nanoparticle. For different values of φ (obtained according to the values of h_x and h_y and the external field H), they obtain a family of straight lines which are the directions in which the *magnetization is in equilibrium*. The magnetization is in *stable* equilibrium when $d^2w/d\varphi^2 > 0$ and in *unstable equilibrium* when $d^2w/d\varphi^2 < 0$.

The *critical* field at which the *irreversible* (*coherent*) *rotation* of the magnetization can be obtained results from the condition

$$\frac{d^2w}{d\varphi^2} = 0, \tag{62}$$

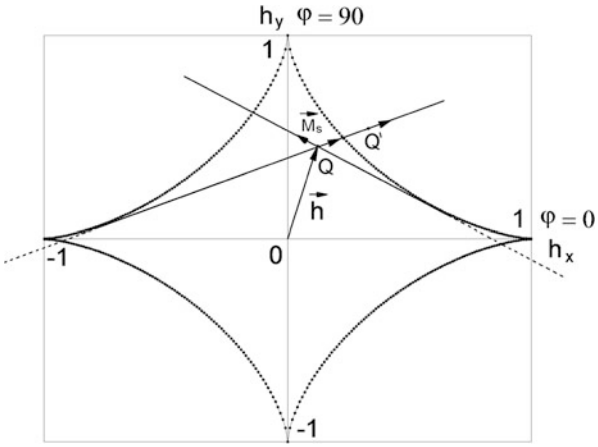

Fig. 16 The astroid in the (h_x0h_y) plan and the magnetization equilibrium directions for $\varphi = 25°$ and $\varphi = 145°$ (computer generated)

which leads to

$$h_x \cos\varphi + h_y \sin\varphi = -\cos(2\varphi). \tag{63}$$

Eliminating the φ in Eqs. 61 and 63, they obtain the *astroid* equation

$$(h_x)^{2/3} + (h_x)^{2/3} = 1, \tag{64}$$

in the plan (h_x0h_y). In Fig. 16, the computer-generated astroid is represented. Also, in the same figure, they represented the lines of equation (61), PC generated for $\varphi = 25°$ and $\varphi = 145°$ (in agreement with Ref. [109]). The continuous part of the straight line corresponds to *the stable state* of the magnetization, and the part discontinuously marked (with dashed lines) corresponds to the *unstable state* (With permission from Eurobit: [84]). In the critical field determined by equation (I.91), a stable equilibrium position determined by a direction moves to another position determined by another direction. Inside the astroid, there are two possible orientations of the vector $\vec{M}_s$, corresponding to the stable positions (see point Q). Outside the astroid, there is only one orientation of $\vec{M}_s$, which corresponds to the stable state (see point Q′). Thus, if in the state Q, the magnetization was oriented in the direction of the figure, by changing the external field in such a way that the point Q is closer to the astroid, the vector $\vec{M}_s$ will rotate smoothly (reversibly, coherently); as soon as the point touches the astroid, the orientation of $\vec{M}_s$ is no longer possible to be (very) close to the previous one direction because that orientation will correspond, from now on, to the unstable state $\left(d^2w/d\varphi^2 < 0\right)$. Therefore, a *rotation by jump* (irreversible) of the magnetization will occur in the direction of minimum energy, a direction for which $d^2w/d\varphi^2 > 0$.

Stoner and Wohlfarth calculated the magnetization (reduced) curves for different angles between the magnetic field and the easy magnetization axis, at

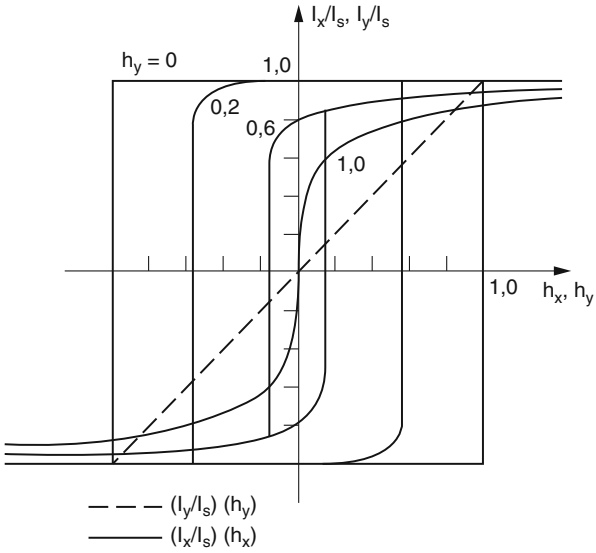

Fig. 17 Theoretical longitudinal magnetization curve $(I_x/I_s)\,(h_x)_{hy\,=\,const.}$ of a uniaxial thin layer. The transversal curve $(I_y/I_s)\,(h_y)_{hx\,=\,0}$ is also shown as *dashed* (Springer [75], Fig. 27.37, © Springer-Verlag 1962. With kind permission from Springer Science and Business Media; Reprinted with permission from [110]. Copyright [1958], AIP Publishing LLC)

magnetization–remagnetization. The curves $M_x/M_s = f(h_x)$ ($M_x = M_s \cos\varphi$, which is the component parallel to the easy magnetization axis) for different constant values of h_y are shown in Fig. 17 (the system is considered a thin layer formed of noninteraction single-domain particles, with uniaxial anisotropy along the layer) (in figure $I \equiv M$).

As shown, the coercive (static) field for coherent rotations, $h_{xr} = H_{xr}/H_{V,u}$, moves from a value 1 to the value 0 when h_y increases from value 0 to value 1. The function $h_{xr} = f(h_y)$ is identical with the critical curve and is given by the astroid equation where h_x must be replaced by h_{xr}. For the magnetization curve $M_y/M_s = f(h_y)$ (component parallel to the hard magnetization axis), when $h_x = 0$, they obtain a *line* (the dashed line shown in Fig. 17). When $h_y = 0$ (which means that external field is applied in the direction x), the magnetization in the direction of easy magnetization follows a *rectangular* hysteresis cycle. This case is very important from a practical point of view, because, (i) on the one hand, in these circumstances, they obtain a switch (very fast reverse to 180°) of the magnetization, by rotation, between two stable states and, (ii) on the other hand, it *enables the determination of the field* (*constant*) *of uniaxial anisotropy achieved by experiment*. Fast switching of the magnetization finds practical application in the production of magnetic memories, such as computer hard drives.

In terms of determining the anisotropy field, imposing the condition $h_x = 1$ (when the irreversible jump at 180° of the magnetization occurs), they obtain the relation

$$H_{V,u} = \frac{2K_u}{\mu_0 M_s} = H_{xr} \cong H_c. \tag{65}$$

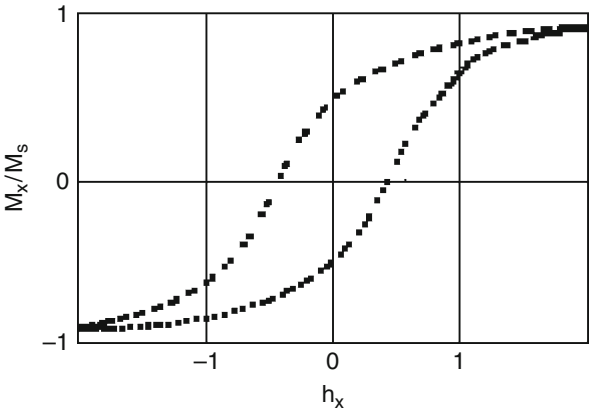

Fig. 18 The hysteresis loop of a system of nanoparticles with the easy magnetization axes randomly oriented (© Eurobit 2004. Reprinted with permission from Ref. [84])

Therefore, the uniaxial anisotropy constant K_u can be determined by measuring experimentally the coercive field H_c, which can be approximated with the critical field at which the rotation by jump of the magnetization takes place.

For a system of *single-domain nanoparticles* with uniaxial anisotropy, in the absence of interactions between them, and with the randomly anisotropy axes, a hysteresis loop is obtained as shown in Fig. 18. In this case [108], the reduced field (h_c)in the direction of magnetization (when the rotations of magnetic moments at unison accurs) is $h_c \cong 0.5$, the mean coercive field is,

$$\langle H_c \rangle \cong \frac{1}{2} H_{V,u} \cong \frac{K_u}{\mu_0 M_s}, \tag{66}$$

(where by $\langle\rangle$ we designated the mean value), and the (theoretical) reduced magnetization is

$$\frac{M_r}{M_s} = 0.5. \tag{67}$$

The results obtained confirm the model [111–113], and only small differences occur in the values $(1/2)H_{V,u}$ and $M_r/M_s = 0.5$, which are slightly lower due to superparamagnetic relaxation effects [18, 33, 102, 114] (which will be discussed in section "Superparamagnetic Behavior of the Nanoparticles") or quantum tunneling of magnetization [115–117] which occurs in the case of small nanoparticles.

When magnetocrystalline anisotropy is different from the uniaxial one, Néel [118] calculated the coercive field for a system of randomly oriented spherical particles, obtaining the value of 0.64 $K_u/\mu_0 M_s$. When the *shape anisotropy* is dominant (see section "Magnetic Anisotropy of Nanoparticles"), considering Eq. 36 and K_{sh}, it results $H_c \sim (N_b - N_a) = N(r)$. For an ensemble of nanoparticles, an extended range of values may exist, so it will be considered $H_c \sim <N(r)>$ (< > mean value) or a function of volume distribution. Other studies [119, 120] showed that the coercive field of the ensemble of nanoparticles is lower than the mean

value, depending on particle size. Of course, this problem is more complex [121]; in reality they must consider the magnetization processes, coherent or noncoherent, that is, the remagnetizations by rotation in unison, the waving of the magnetization or magnetization curving that may exist depending on the shape and size of the sample, as well as the existence of other forms of anisotropy (see section "Magnetic Anisotropy of Nanoparticles").

Single-Domain Nanoparticles in the Area of Sizes Where Fluctuations in Magnetization Exist: The Coercive Field of Nanoparticles

In the presence of thermal activation ($T > 0$) (With permission from Eurobit: [84]), when the nanoparticle's volume becomes lower than V_t ($V < V_t$) (see Fig. 1), the magnetization of nanoparticle fluctuates along the easy magnetization axis (reversing at 180°) (Néel) [122]. For the spontaneous magnetization to reverse, in the absence of external magnetic field ($H = 0$), considering nanoparticle with uniaxial magnetic anisotropy (see section "Magnetic Anisotropy of Nanoparticles")

$$W_{V,u} = K_u V \sin^2\varphi, \tag{68}$$

the energy barrier must be overcome:

$$W_b = K_u V \tag{69}$$

($\varphi = \pi/2$) (Fig. 19a). In this case, there is some probability of crossing the potential barrier [123, 124] which is greater as the temperature is higher and the nanoparticle's volume lower.

The time in which this process takes place [125] is the *Néel relaxation time* [122]:

$$\tau_N = \tau_0 \exp\left(\frac{K_u V}{k_B T}\right), \tag{70}$$

where τ_0 is a time constant which usually has the value 10^{-9} s [126], and the process is known as Néel magnetic relaxation. In practical conditions of measurement, the interval of time in which the relaxation process is registered is called *measurement time* (t_m). In the case of static measurements, it is considered 100 s [123]. At limit, when the relaxation time is equal to the measuring time ($\tau_N = t_m$), there can be found the nanoparticle's volume corresponding to the *transition* from the state in which the magnetization does not relax (magnetization is stable over time) to the state in which the magnetization relaxes (it reverses by 180° in a certain time). Thus, from Eq. 70

$$K_u V_t \cong 25 k_B T, \tag{71}$$

results and the *threshold* volume

$$V_t = \frac{25 k_B T}{K_u}. \tag{72}$$

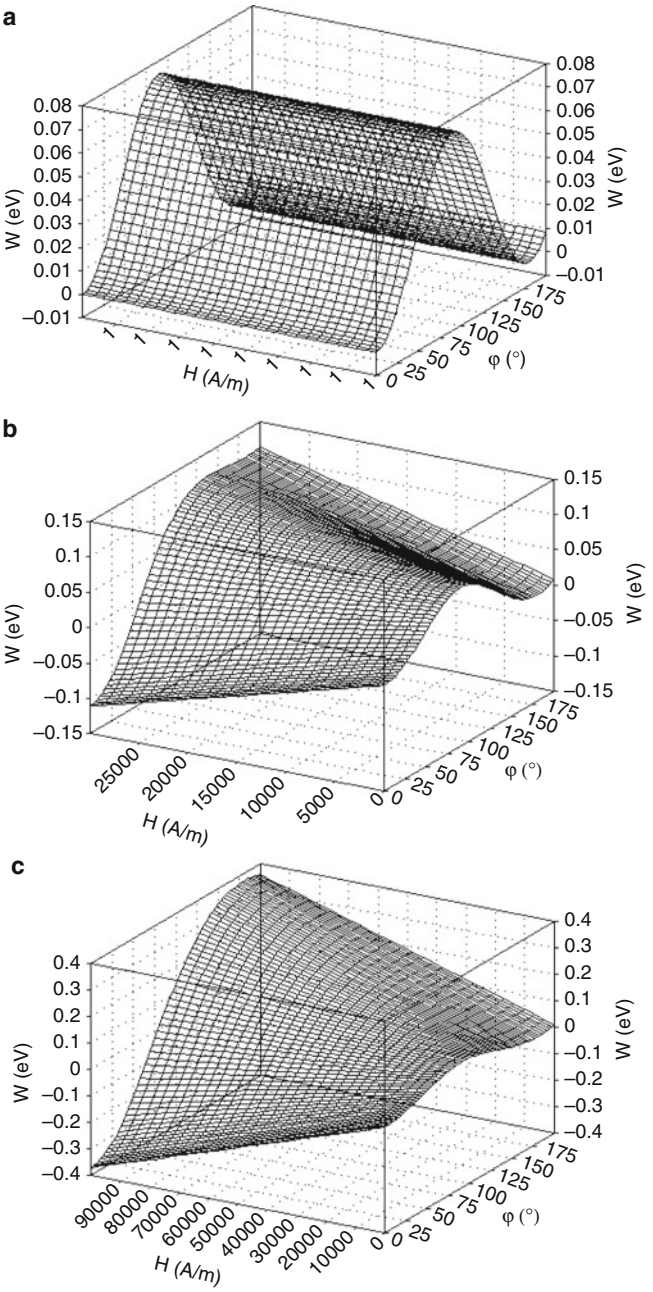

Fig. 19 (**a**) Variation of the nanoparticle's energy (expressed in eV) as a function of the angle φ and the field H, for $H = 1\ \mathrm{Am}^{-1}$ (**a**) and when H increases: from 1 to the maximum value H_m, i.e., $30 \times 10^3\ \mathrm{Am}^{-1}$ (**b**) and $100 \times 10^3\ \mathrm{Am}^{-1}$ (**c**), respectively [130] ()

Also, it defines a temperature corresponding to the blocking of magnetic moments (*blocking temperature*) [123]:

$$T_b = \frac{K_u V}{25 k_B}. \tag{73}$$

When the nanoparticle with volume V has a temperature $T < T_b$, the magnetic moment of the nanoparticle is blocked, and when $T > T_b$, the magnetic moment of nanoparticle fluctuates along the axis of easy magnetization (it relaxes). In conditions of *dynamic* measurement, commonly used in current practice (using, e.g., the Mössbauer spectroscopy [12, 127, 128], where the measuring time is 5×10^{-8} s), considering the experimental time of measurement, corresponding to the technique used, formulas (71) and (73) can be considered general [129]

$$V_t = \frac{k_B T}{K_u} \ln(t_m/\tau_0), \tag{74}$$

respectively,

$$T_b = \frac{K_u V}{k_B \ln(t_m/\tau_0)}. \tag{75}$$

In the *presence of an external magnetic field* applied along the easy magnetization direction of nanoparticles, the energy barrier will change (W_{bH}) [130], either by increasing or decreasing, depending on the sense of the magnetic field (increases when the field H is applied in the sense of magnetization M_s and decreases in reverse). In Fig. 19 (b, c), the variation of the energy barrier for Fe_3O_4 nanoparticles surfacted with oleic acid and dispersed in kerosene (ferrofluid) [130], having the magnetic diameter of 12.35 nm [71] and a uniaxial anisotropy constant $K_u = 12.2 \times 10^3$ Jm^{-3}, is shown [19].

When the magnetic field is applied in the opposite direction of spontaneous magnetization, starting from the energy of the particle in the field, they obtain the formula [131]

$$W_{bH} = K_u V_m \left(1 - \frac{\mu_0 m_{m,NP} H}{2 K_u V_m}\right)^2, \tag{76}$$

where the magnetic moment of the nanoparticle has been replaced (see section "Magnetic Behavior of Nanoparticles in an External Field"), considering the observations made in section "Surface Spin Disorder in Nanoparticles and Saturation Magnetization." In this case, in agreement with the formula (71), it results that there will be a certain external field, called *critical field* (or threshold field, H_{ct}), at

which the magnetic moment will reverse to 180°. This can be determined by imposing the condition (Eq. 71)

$$K_u V_m \left(1 - \frac{\mu_0 m_{m,NP} H_{ct}}{2K_u V_m}\right)^2 = 25 k_B T, \tag{77}$$

from where it results

$$H_{ct} = \frac{2K_u V_m}{\mu_0 m_{m,NP}} \left(1 - \sqrt{\frac{25 k_B T}{K_u V_m}}\right) = H_{V,u} \left(1 - \sqrt{\frac{25 k_B T}{K_u V_m}}\right). \tag{78}$$

In the absence of thermal activation (when the temperature is $T = 0$), from Eq. (78) results the formula $H_{ct} = H_{V,u}$, meaning that the critical field becomes equal to the anisotropy field (see Eq. 65), a formula in agreement with the S-W model (see section "Single-Domain Nanoparticles with Stable Magnetization"). Given the formula for the threshold volume (Eq. 72) and using Eq. 78, the end result is

$$H_{ct} = H_{V,u} \left[1 - \left(\frac{V_{mt}}{V_m}\right)^{1/2}\right] = H_{V,u} \left[1 - \left(\frac{D_{mt}}{D_m}\right)^{3/2}\right], \tag{79}$$

where V_{mt} is the threshold magnetic volume and D_{mt} is the threshold magnetic diameter, respectively, in the approximation of the spherical nanoparticle. Using Eq. 73, the formula (79) can also be written according to blocking temperature:

$$H_{ct} = H_{V,u} \left[1 - \left(\frac{T}{T_b}\right)^{1/2}\right]. \tag{80}$$

This result (Eq. 79) shows that the critical field (coercive field in this case) decreases as the magnetic diameter of the nanoparticles decreases, and becomes zero at the threshold diameter ($D_m = D_{mt}$). Experimental results broadly confirm the law of variation (Eq. 79) in the range $D_m/D_{mt} = (1 - 5)$. Kneller and Luborsky [132] found a good concordance between the calculated and experimental values for an ensemble of spherical nanoparticles of CoFe. For values $D_m = (5 - 6)D_{mt}$, deviations from this pattern occur, the coercive field decreasing in this area, approaching the coercive field characteristic to the bulk material.

For a system of identical nanoparticles (in the absence of interactions) in the case of random orientation of uniaxial anisotropy axis, they will use Eq. 66 for the anisotropy field $H_{V,u}$.

In Fig. 20 the variation of coercive field of nanoparticles according to their magnetic diameter, starting from the area with the magnetic domain structure (very large nanoparticles (tens to hundreds of nm)) until the superparamagnetic area (very small nanoparticles (a few nm)) is shown, qualitatively. Here, it should be specified that such a variation is obtained for nanoparticles with low anisotropy and at usual

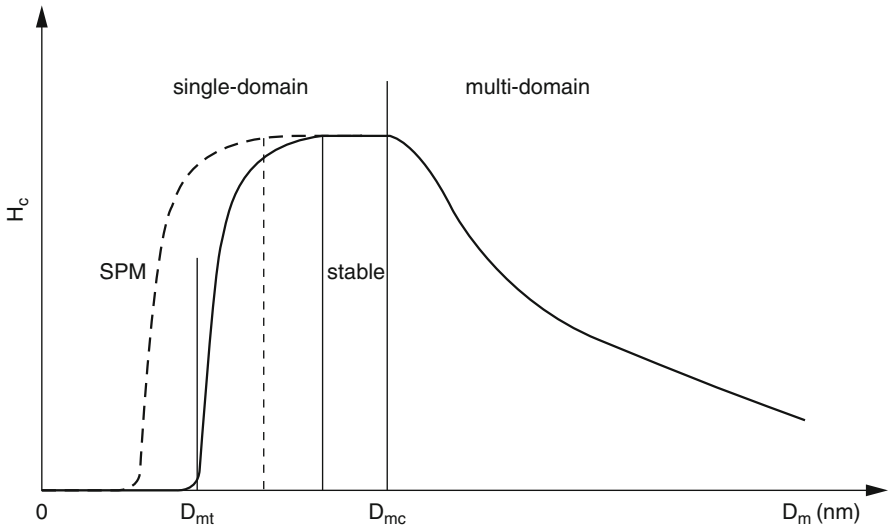

Fig. 20 The variation of the coercive field of a system of nanoparticles according to their magnetic diameter

temperatures (e.g., room temperature) when there are thermal fluctuations of spontaneous magnetization (magnetic moments) of single-domain nanoparticles.

The single-domain area with *stable* magnetization, quite narrow, close to the critical diameter, for $D_m < D_{mc}$, can be extended to lower values of nanoparticle diameter (see dashed curve) by the following means: (i) *reducing the temperature*, possibly to 0 K ($T \rightarrow 0$, under the conditions of the S-W model), or (ii) at room temperature by *increasing the magnetic anisotropy*. Case (ii) can be obtained using nanoparticles with very high anisotropy (hard), e.g., Co ferrite nanoparticles. Noting in Eq. 79

$$\sigma = \frac{K_u V_m}{k_B T}, \tag{81}$$

when $\sigma >> 1$, τ_N is very high and the magnetic moments of nanoparticles are "frozen" on the uniaxial anisotropy axes. In this case, and in normal conditions, the magnetization is stable.

A variation similar to that of Fig. 20, continuous curve, was found in the case of soft Ni-Zn ferrite nanoparticles (the anisotropy constant is 1.5×10^3 Jm^{-3}) [5], where the area of stability of magnetization ($H_c \sim$ constant) is virtually absent at room temperature (Fig. 21). In this case, besides the low anisotropy and high temperature (room temperature) at which the measurement of the coercive field was made, the variation is also influenced by the existence of a *distribution* of diameters of the nanoparticles from the sample (in small nanoparticles the spontaneous magnetization fluctuates along the easy magnetization axis).

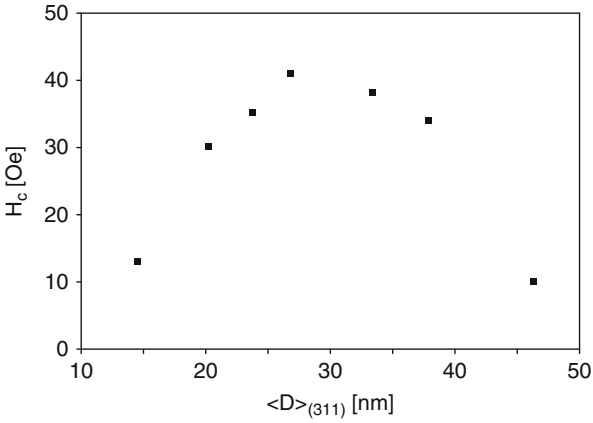

Fig. 21 Coercivity as a function of the average diameter of nanocrystallites [5] (© IOP Publishing. Reproduced by permission of IOP Publishing. All rights reserved)

It should be noted that some discrepancies between the calculated (Eq. 79 or 80) and experimental values [133–137] are due to the effects presented in sections "Saturation Magnetization of Nanoparticles" and "Magnetic Anisotropy of Nanoparticles," regarding decreases of the saturation magnetization and increases of magnetic anisotropy for nanoparticles, which can dramatically change the magnetic behavior.

Superparamagnetic Behavior of the Nanoparticles

In the area of small diameters, where $D_m < D_{mt}$ (generally less than 10 nm for nanoparticles with moderate anisotropy), and at room temperature (~300 K), when the condition $\sigma > 1$ is met and σ slightly greater than 1 (Eq. 81), the relaxation time of the magnetic moments of the nanoparticles, oriented or not, is very small, of the order of 10^{-9} s. Under these conditions, the magnetization of single-domain nanoparticles fluctuates rapidly along the easy magnetization axis [122], being always in thermodynamic equilibrium, and when applying an external magnetic field, it follows, almost instantly, the field variations. This system, from a magnetic point of view, behaves like a system of paramagnetic atoms (Langevin) [138], in the absence of interactions, where the atomic magnetic moment exists instead of the nanoparticle magnetic moment. Having in view this basic feature between this two paramagnetic systems, atoms or nanoparticles (which contains $>10^5$ atoms) with their magnetic moments (atomic magnetic moment for paramagnetic atom ($\vec{\mu}_a$) and nanoparticle magnetic moment ($\vec{m}_{m,NP}$) for nanoparticle (see section "Magnetic Behavior of Nanoparticles in an External Field"), in this case the system of nanoparticles was called superparamagnetic (SPM) [129], and the behavior in the external field, *superparamagnetic behavior*. Under these conditions for the magnetization of the nanoparticle system, the atomic paramagnetism theory of Langevin applies [138].

Thus, the magnetization of a SPM nanoparticle system is given by the formula [139]

$$M_{SPM}(H,T) = nm_{m,NP}\left(cth\frac{\mu_0 m_p H}{k_B T} - \frac{k_B T}{\mu_0 m_p H}\right), \tag{82}$$

where n is the concentration of nanoparticles in the system, $m_{m,NP}$ is the magnetic moment of the nanoparticle, and the parenthesis contains the Langevin function

$$L(H,T) = cth\frac{\mu_0 m_{m,NP} H}{k_B T} - \frac{k_B T}{\mu_0 m_{m,NP} H}. \tag{83}$$

The magnetization as a function of magnetic field, $M_{SPM}(H,T) = f(H)_T$, is without hysteresis loop ($H_c = 0$), and the curve of first magnetization (for $H > 0$) not having an inflection point, being defferent from that of the other nanoparticles, ferro- or ferrimagnetic, single-domain, stable or less stable, or with a magnetic domain structure, where there is always a hysteresis loop (small ar large) and with an inflection point in their first magnetization curve in a static external magnetic field (see sections "Hysteresis Magnetic Behavior of Multi-domain Nanoparticles" and "Single-Domain Nanoparticles with Stable Magnetization"). For a system of nanoparticles to have a superparamagnetic behavior in the external field, in the absence of interactions, two conditions must be met: (i) the magnetization curves $M = f(H)$ recorded at different temperatures must be without hysteresis and follow the Langevin function, and (ii) the same magnetization curves in the representation $M/M_{sat} = f(H/T)$ should overlap.

In reality, there is a size distribution of nanoparticles in a system; therefore, for a rigorous approach, their distribution function should also be considered. In most cases, it was found that the nanoparticle distribution is lognormal [140–143],

$$f(D) = \frac{1}{\sqrt{2\pi}\lambda D}\exp\left\{-\frac{[\ln(D) - \ln(D_0)]^2}{2\lambda^2}\right\}, \tag{84}$$

where D_0 and λ are distribution parameters. In these conditions, the magnetization of the nanoparticle system will be

$$M_{SPM} = M_{sat}\int_0^\infty L[\xi(H,T,D_m)]f(D_m)d(D_m), \tag{85}$$

where the argument of the Langevin function is

$$\xi(H,T,D_m) = \frac{\pi}{6}\frac{\mu_0 D_m^3 M_s H}{k_B T}, \tag{86}$$

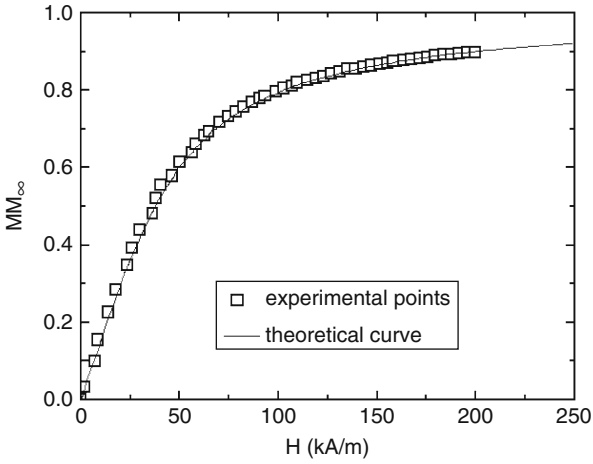

Fig. 22 Reduced magnetization curve of the nanocomposite $(Zn_{0.15}Ni_{0.85}Fe_2O_4)_{0.15}/(SiO_2)_{0.85}$ registered at room temperature and 50 Hz frequency of the magnetization field (H) (Reprinted from [18], Copyright (2007), with permission from Elsevier)

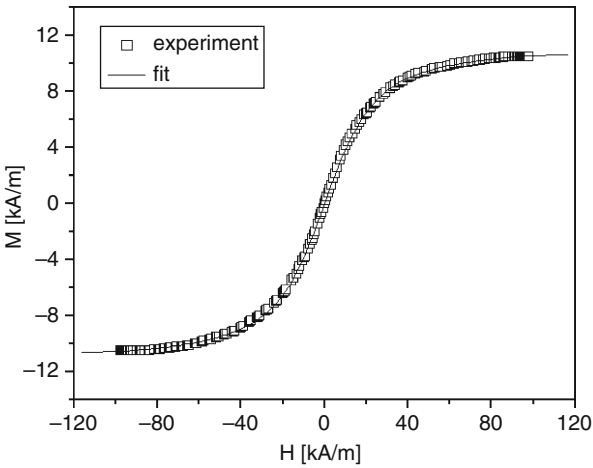

Fig. 23 Magnetization curve at room temperature [71] (© IOP Publishing. Reproduced by permission of IOP Publishing. All rights reserved)

in the approximation of spherical nanoparticles. In formula (85) it was taken into account Eq. 5 for the saturation magnetization of the system of nanoparticles and Eq. 23 for the diameter of the magnetic nanoparticles (given that $D_m < D$ (8), as shown in the section "Surface Spin Disorder in Nanoparticles and Saturation Magnetization").

In Fig. 22 the first magnetization (reduced) curve for Ni-Zn nanoparticles isolated in a SiO_2 amorphous matrix (nanocomposite), having a concentration of 15 % and the mean magnetic diameter $< D_m > = 8.9$ nm [18], is shown, and in Fig. 23 the magnetization–remagnetization curve of the Fe_3O_4 nanoparticles covered with oleic acid and dispersed in kerosene (nanofluid), with mean magnetic diameter of 10.9 nm and the narrow lognormal distribution of their sizes, is shown [71]. The continuous line represents the fitting to the Langevin function. The analysis of the curves obtained experimentally, in the area of *low fields* ($\xi << 1$)

and *high fields* ($\xi >> 1$) [71, 144], enables the determination of the distribution parameters (D_0 and λ) and then of the mean *magnetic* diameter of the nanoparticles in the system,

$$\langle D_m \rangle = D_0 \exp\left(\lambda^2/2\right). \tag{87}$$

This is a very important issue for the magnetic nanoparticles because it allows the evaluation of the *thickness of the surface layer of the nanoparticles* (for SPM behavior), knowing that $D_m < D$ (see section "Saturation Magnetization of Nanoparticles") in various cases (small nanoparticles, surfacted nanoparticles, nanoparticles embedded in various matrices, etc.), using electron microscopy (TEM or HR-TEM) [20, 145] or other techniques, such as Small Angle Neutron Scattering (SANS), etc., to determine the physical diameter (D). Given that the thickness of the nanoparticles' surface layer is of the order of 1 nm [18, 19, 32], the two diameters (magnetic and physical) must be determined with high accuracy. Therefore, in a more accurate analysis, especially in the case of broad distribution of nanoparticle diameters, for the determination of the mean magnetic diameter, it must be taken into account that the magnetic moment of the nanoparticle also depends on the magnetic diameter,

$$m_{m,NP}(D_m) = \pi M_s D_m^3/6. \tag{88}$$

In this case, for the magnetization of the nanoparticle system, function will be used [71, 146]:

$$M_{SPM} = n \int_0^\infty m_p(D_m) L[\xi(H,T,D_m)] f(D_m) d(D_m), \tag{89}$$

instead of the one given by Eq. 85.

Conclusion

The finite size of nanoparticles is a critical parameter that, according to its value, leads to a certain magnetic structure: multi-domain, with nonuniform magnetization, or single domain, with uniform and stable magnetization or with fluctuant magnetization. Consequently, the nanoparticles will have a certain magnetic behavior in the external magnetic field, from ferro- or ferrimagnetic with large hysteresis loop, for big-sized nanoparticles (tens to hundreds of nm), similar to the bulk, to a behavior with no hysteresis, for smaller sizes, and, respectively, to a superparamagnetic behavior for very small-sized nanoparticles (a few nm).

The size of nanoparticles is also reflected in the structure of the spins (magnetic atomic moments) from the surface of the nanoparticles, which are no longer aligned under the action of the exchange or superexchange interaction (being placed in a

disorder structure), with the spins from the core of the nanoparticles, which are ferro- or ferrimagnetically aligned, a structure that becomes dominant in the case of small-sized nanoparticles, causing a considerable decrease of the saturation magnetization of nanoparticles. Consequently, they must take into consideration a model for the core–shell nanoparticles: core, where the magnetic moments are aligned, and shell, where the magnetic moments are in a disorder structure. The noncollinearity of the spins from the surface of the nanoparticles is reflected in the decrease of the saturation magnetization of the nanoparticles, as compared to that of the corresponding bulk material, the effect being more intense when the nanoparticles are smaller (a few nm). Furthermore, the decrease of the saturation magnetization is higher in the case of ferrimagnetic nanoparticles, where the exchange interaction, which aligns the atomic magnetic moments, takes place through the ions of oxygen (superexchange interaction).

The effect of the size decrease of nanoparticles also reflects upon the variation of the saturation magnetization of nanoparticles as a function of temperature, which is different from that of the corresponding bulk material, in the case of many nanostructures. Also, the Curie temperature of nanoparticles decreases along with the decrease of their size, the decrease being more pronounced when the nanoparticles are smaller, in the range of nanometers.

The magnetic anisotropy also modifies in the case of nanoparticles, in some cases becoming unusually high, as compared to the magnetocrystalline anisotropy of the corresponding bulk material, especially in the case of small nanoparticles (a few nm). An important contribution to the magnetic anisotropy is due to the surface anisotropy component, which may even become dominant in the case of small nanoparticles, as compared to the magnetocrystalline anisotropy or to the shape anisotropy. Besides the nature of the material, the value of this contribution also depends on the nanoparticles being surfactant or not or embedded in different crystalline or amorphous matrices. When the nanoparticles are embedded in matrices, very high magnetic anisotropies may occur, one or two orders of magnitude higher than the magnetocrystalline anisotropy, due to the contribution of anisotropy determined by tensions (stress anisotropy).

All these aspects must be taken into consideration for the accurate fundamental study of the magnetic properties of nanoparticles and their practical future applications in nanotechnology.

References

1. H. Kachkachi, J. Magn. Magn. Mater. **316**, 248 (2007)
2. T. Kim, M. Shima, J. Appl. Phys., **101**, 09 M516 (2007)
3. R.H. Kodama, J. Magn. Magn. Mater. **200**, 359 (1999)
4. L. Zhang, G.C. Papaefthymiou, R.F. Ziolo, J.Y. Ying, Nano Struct Mater **9**, 185 (1997)
5. C. Caizer, M. Stefanescu, J. Phys. D Appl. Phys. **35**, 3035 (2002)
6. C. Caizer, Mater Sci. Eng. B **100**, 63 (2003)
7. A.E. Berkowitz, W.J. Schuele, P.J. Flanders, J. Appl. Phys. **39**, 1261 (1968)
8. J.M.D. Coey, Phys. Rev. Lett. **27**, 1140 (1971)

9. A.E. Berkowitz, J.A. Lahut, I.S. Iacobs, L.M. Levinson, D.W. Forester, Phys. Rev. Lett. **34**, 594 (1975)
10. A.E. Berkowitz, J.A. Lahut, C.E. VanBuren, IEEE Trans. Magn. **MAG-16**, 184 (1980)
11. R.H. Kodama, A.E. Berkowitz, E.J. McNiff, S. Foner, Phys. Rev. Lett. **77**, 394 (1996)
12. C. Cannas, G. Concas, A. Musinu, G. Piccaluga, G. Spano, Z. Naturforsch **54 a**, 513 (1999)
13. E. Tronc, A. Ezzir, R. Cherkaoui, C. Chanéac, M. Noguès, H. Kachkachi, D. Fiorani, A.M. Testa, J.M. Grenèche, J.P. Jolivet, J. Magn. Magn. Mater. **221**, 63 (2000)
14. A.H. Morrisch, K. Haneda, J. Appl. Phys. **52**, 2496 (1981)
15. D. Lin, A.C. Nunes, C.F. Majkrzak, A.E. Berkowitz, J. Magn. Magn. Mater. **145**, 343 (1995)
16. R.V. Upadhyay, D. Srinivas, R.V. Mehta, J. Magn. Magn. Mater. **214**, 105 (2000)
17. C. Cannas, D. Gatteschi, A. Musinu, G. Piccalunga, C. Sangregorio, J. Phys. Chem. B **102**, 7721 (1998)
18. C. Caizer, J. Magn. Magn. Mater. **320**, 1056 (2008)
19. I. Hrianca, C. Caizer, Z. Schlett, J. Appl. Phys. **92**, 2125 (2002)
20. C. Caizer, M. Popovici, C. Savii, Acta Mater. **51**, 3607 (2003)
21. A.E. Berkowitz, R.H. Kodama, S.A. Makhlouf, F.T. Parker, F.E. Spada, E.J. McNiff Jr., S. Foner, J. Magn. Magn. Mater. **196–197**, 591 (1999)
22. P. Mollard, P. Germi, A. Rousset, Physica B **86–88**, 1393 (1977)
23. B. Martinez, A. Roig, E. Molins, T. González-Carreño, C.J. Serna, J. Appl. Phys. **83**, 3256 (1998)
24. Y.T. Jeon, J.Y. Moon, G.H. Lee, Int. J. Mod. Phys. B **20**, 4390 (2006)
25. A. Millan, A. Urtizberea, N.J.O. Silva, F. Palacio, V.S. Amaral, E. Snoeck, V. Serin, J. Magn. Magn. Mater. **312**, L5 (2007)
26. P. Guardia, B. Batlle-Brugal, A.G. Roca, O. Iglesias, M.P. Morales, C.J. Serna, A. Labarta, X. Batlle, J. Magn. Magn. Mater. **316**, e756 (2007)
27. Y. Ichiyanagi, T. Uehashi, S. Yamada, Y. Kanazawa, T. Yamada, J. Therm. Anal. Calorim. **81**, 541 (2005)
28. D.T.T. Nguyet, N.P. Duong, L.T. Hung, T.D. Hien, T. Satoh, J. Alloys Compd. **509**, 6621 (2011)
29. S. Arajs, L.C. Nanna, D.H. Rasmussen, R.L. Bush, J. Appl. Phys. **67**, 4499 (1990)
30. J.P. Chen, C.M. Sorensen, K.J. Klabunde, G.C. Hadjipanayis, E. Devlin, A. Kostikas, Phys. Rev. B **54**, 9288 (1996)
31. C. Rocchiccioli-Deltcheff, R. Franck, V. Cabuil and R. Massart, J. Chem. Res. (S) 5, 126 (1987)
32. R.E. Rosensweig, *Ferrohydrodynamics* (Cambridge University Press, Cambridge, 1985)
33. Yu.L. Raikher, M.I. Shliomis, Adv. Chem. Phys., **87**, 8 (1994)
34. C. Caizer, J. Magn. Magn. Mater. **251**, 304 (2002)
35. C. Caizer, I. Hrianca, Ann. Phys. **12**, 115 (2003)
36. C. Caizer, I. Hrianca, Eur. Phys. J. B. **31**, 391 (2003)
37. H. Jacobsen, K. Lefmann, E. Brok, C. Frandsen, S. Mørup, J. Magn. Magn. Mater, **324**, 3218 (2012)
38. C. Vázquez-Vázquez, M.A. López-Quintela, M.C. Buján-Núñez, J. Rivas, J. Nanopart. Res. **13**, 1663 (2011)
39. K. Mandal, S. Mitra, P.A. Kumar, Europhys. Lett. **75**, 618 (2006)
40. C. Caizer, Appl. Phys. A **80**, 1745 (2005)
41. S. Mørup, B.R. Hansen, Phys. Rev. B **72**, 024418 (2005)
42. M.D. Kuz'min, A.M. Tishin, Phys. Lett. A **341**, 240 (2005)
43. G.F. Goya, T.S. Berquó, F.C. Fonseca, J. Appl. Phys. **94**, 3520 (2003)
44. J. Wang, W. Wu, F. Zhao, G. Zhao, Appl. Phys. Lett. **98**, 083107 (2011)
45. H.M. Lu, Z.H. Cao, C.L. Zhao, P.Y. Li, X.K. Meng, J. Appl. Phys. **103**, 123526 (2008)
46. W. Wu, X. Lin, H. Duan, J. Wang, Int. J. Mod. Phys. B **26**, 1250073 (2012)
47. Xe. He, H. Shi, Particuology, **10**, 497 (2012)
48. H. Mayama, T. Naito, Physica E **41**, 1878 (2009)

49. N.S. Gajbhiye, G. Balaji, M. Ghafari, Phys. Status Solidi A **189**, 357 (2002)
50. M.E. Fisher, A.E. Ferdinand, Phys. Rev. Lett. **19**, 169 (1967)
51. F. Huang, G.J. Mankey, M.T. Kief, R.F. Willis, J. Appl. Phys. **73**, 6760 (1993)
52. K. Chen, A.M. Ferrenberg, D.P. Landau, Phys. Rev. B **48**, 3249 (1993)
53. J. Mazo-Zuluaga, J. Restrepo, J. Mejia-Lopez, J. Phys. Condens. Matter **20**, 195213 (2008)
54. F. Bloch, Z Phys **61**, 206 (1930)
55. A.H. Eschenfelder, in: Landolt-Börnstein, *Magnetic properties I* (Springer, Berlin, 1962)
56. A.T. Aldred, P.H. Frohle, Int. J. Magnet. **2**, 195 (1972)
57. A.T. Aldred, Phys. Rev. B **11**, 2597 (1975)
58. J.F. Dillon, in Landolt-Börnstein, *Magnetic properties I* (Springer, Berlin, 1962)
59. P.V. Hendriksen, S. Linderoth, P.A. Lindgard, J. Magn. Magn. Mater. **104–107**, 1577 (1992)
60. S. Linderoth, L. Balcells, A. Labarta, J. Tejada, P.V. Hendriksen, S.A. Sethi, J. Magn. Magn. Mater. **124**, 269 (1993)
61. P.V. Hendriksen, S. Linderoth, P.A. Lindgard, Phys. Rev. B **48**, 7259 (1993)
62. C. Caizer, *Habil. Thesis* (2013)
63. C. Caizer, Solid State Commun. **124**, 53 (2002)
64. A.H. Eschenfelder, J. Appl. Phys. **29**, 378 (1958)
65. B. Berkovsky, V. Bashtovoy, *Magnetic Fluids and Applications Handbook* (Begell House, New York, 1996)
66. M. Xu, P.J. Ridler, J. Appl. Phys. **82**, 326 (1997)
67. Yu.I. Raikher, M.I. Shliomis, Adv. Chem. Phys., **87**, 3 (1994)
68. R.V. Upadhyay, D. Srinivas, R.V. Mehta, J. Magn. Magn. Mater. **214**, 105 (2000)
69. M.D. Sastry, Y. Babu, P.S. Goyal, R.V. Mehta, R.V. Upadhyay, D. Srinivas, J. Magn. Magn. Mater. **149**, 64 (1995)
70. E. Tronc, A. Ezzir, R. Cherkaoui, C. Chanéac, M. Noguès, H. Kachkachi, D. Fiorani, A.M. Testa, J.M. Grenèche, J.P. Jolivet, J. Magn. Magn. Mater. **221**, 63 (2000)
71. C. Caizer, J. Phys. Condens. Matter **15**, 765 (2003)
72. K. Honda, S. Kaya, Sci. Rep. Tohoku Univ. **15**, 721 (1926)
73. S. Kaya, Sci. Rep. Tohoku Univ. **17**, 639 (1928)
74. S. Kaya, Sci. Rep. Tohoku Univ. **17**, 1157 (1928)
75. E. Kneller, *Ferromagnetismus* (Springer, Berlin, 1962)
76. H.C. Akulov, Zs. Phys. **52**, 389 (1928)
77. G. Aubert, J. Appl. Phys. **39**, 504 (1968)
78. W.J. Carr, *Handbook of Phys*., **XVIII**, 274 (1960)
79. C. Kittel, J.H. van Vleck, Phys. Rev. **118**, 1231 (1960)
80. L. Neel, Compt. Rend. **237**, 1613 (1953)
81. L. Neel, J. Phys. Radium **15**, 225 (1954)
82. F. Bødker, S. Mørup, S. Linderoth, Phys. Rev. Lett. **72**, 282 (1994)
83. C. Papusoi, J. Magn. Magn. Mater. **195**, 708 (1999)
84. C. Caizer, *Magnetic Nanofluids (in Romanian)* (Eurobit Publishing House, Timisoara, 2004)
85. F. Gazeau, J.C. Bacri, F. Gendron, R. Perzynski, L. Raikher Yu, V.I. Stepanov, E. Dubois, J. Magn. Magn. Mater. **186**, 175 (1998)
86. A. van Broese Groenou, J.A. Schulkes, D.A. Annis, J. Appl. Phys **38**, 1133 (1967)
87. J.K. Vassiliou, V. Mehrotra, M.W. Russell, E.P. Giannelis, J. Appl. Phys. **73**, 5109 (1993)
88. J.M.D. Coey, D. Khalafalla, Phys. Status Solidi A **11**, 229 (1972)
89. A.H. Morrish, E.P. Valstyn, J. Phys. Soc. Jpn. **17**, 392 (1962)
90. S. Mørup, J. Magn. Magn. Mater. **37**, 39 (1983)
91. V. Skumryev, S. Stoyanov, Y. Zhang, G. Hadjipanayis, D. Givord, J. Nogués, Nature **423**, 850 (2003)
92. R.H. Kodama, A.E. Berkowitz, Phys. Rev. B **50**, 0321 (1999)
93. H. Kachkachi, M. Dimian, Phys. Rev. B **66**, 174419 (2002)
94. H. Kachkachi, E. Bonet, Phys. Rev. B **73**, 224402 (2006)

95. M. Jamet, W. Wernsdorfer, C. Thirion, V. Dupuis, P. Mélinon, A. Pérez, D. Mailly, Phys. Rev. B **69**, 024401 (2004)
96. E. De Biasi, R.D. Zysler, C.A. Ramos, H. Romero, D. Fiorani, Phys. Rev. B **71**, 104408 (2005)
97. J. Mazo-Zuluaga, J. Restrepo, J. Mejía-López, J. Appl. Phys. **103**, 113906 (2008)
98. A. Hubert, R. Schäfer, *Magnetic Domains* (Springer, Berlin, 1998)
99. E. Becker, H. Polley, Ann. Phys. **37**, 534 (1940)
100. R. Grossinger, Phys. Status Solidi A **66**, 665 (1981)
101. C. Caizer, V. Tura, J. Magn. Magn. Mater. **301**, 513 (2006)
102. H. Kojima, in *Ferromagnetic Materials* ed. by E.P. Wohlfarth (North-Holland, Amsterdam, 1982)
103. C. Kittel, Phys. Rev. **70**, 965 (1946)
104. L. Neel, Compt. Rend. Acad. Sci. Paris, **224**, 1488 and 1550 (1947)
105. C. Kittel, Rev. Mod. Phys. **21**, 541 (1949)
106. C. Caizer, M. Stefanescu, Physica B **327**, 129 (2003)
107. L. Landau, E. Lifshitz, Phys. Z. S. **8**, 153 (1935)
108. E.C. Stoner, E.P. Wohlfarth, Philos. Trans. R. Soc. Lond. A, **240**, 599 (1948)
109. J.C. Slonkzewski, Research Memo., IBM Research Center, N.Y. (1956, unpublished)
110. D.O. Smith, J. Appl. Phys. **29**, 264 (1958)
111. W. Wernsdorfer, C. Thirion, N. Demoncy, H. Pascard, D. Mailly, J. Magn. Magn. Mater. **242–245**, 132 (2002)
112. A. Stancu, L. Spinu, IEEE Trans. Magn. **34**, 3867 (1998)
113. A. Stancu, I. Chiorescu, IEEE Trans. Magn. **33**, 2573 (1997)
114. B.D. Cullity, *Introduction to Magnetic Materials* (Addison-Wesley, Reading, 1972)
115. W. Wernsdorfer et al., Phys. Rev. Lett. **79**, 4014 (1997)
116. E.M. Chudnovsky, L. Gunther, Phys. Rev. Lett. **60**, 661 (1988)
117. E.M. Chudnovsky, J. Tejada, *Macroscopic Quantum Tunneling of the Magnetic Moment* (Cambridge University Press, Cambridge, 1998)
118. L. Neel, C. R. Acad. Sci. Paris, **224**, 1488 and 1550 (1947)
119. C.P. Bean, J. Appl. Phys. **26**, 1381 (1955)
120. R.B. Campbell, J. Appl. Phys. **28**, 381 (1957)
121. B. Barbara, *Magnetization Reversal of Nano-particles* (Springer, Berlin-Heidelberg, 2001) (in: E. Beaurepaire, F. Scheurer, G. Krill and J.P. Kappler (Eds.): LNP **565**, 157 (2001))
122. L. Néel, Ann. Geophys. **5**, 99 (1949)
123. L. Néel, Adv. Phys. **4**, 191 (1955)
124. W.F. Brown, J. Appl. Phys. **30**, 130S (1959)
125. A. Aharoni, Phys. Rev. A **135**, 447 (1964)
126. C.H. Back, D. Weller, J. Heidmann, D. Mauri, D. Guarisco, E.L. Garwin, H.C. Siegmann, Phys. Rev. Lett. **81**, 3251 (1998)
127. J.L. Dormann, F. D'Orazio, F. Lucari, E. Tronc, P. Prené, J.P. Jolivet, D. Fiorani, R. Cherkaoui, M. Nogués, Phys. Rev. B **53**, 14291 (1996)
128. J.L. Dormann, L. Spinu, E. Tronc, J.P. Jolivet, F. Lucari, F. D'Orazio, D. Fiorani, J. Magn. Magn. Mater. **183**, L255 (1998)
129. C.P. Bean, L.D. Livingston, J. Appl. Phys. **30**, 120S (1959)
130. C. Caizer, J. Phys. Condens. Matter **17**, 2019 (2005)
131. C.L. Dennis, R.P. Borges, L.D. Buda, U. Ebels, J.F. Gregg, M. Hehn, E. Jouguelet, K. Qunadjela, I. Petej, I.L. Prejbeanu, M.J. Thornton, J. Phys. Condens. Matter **14**, R1175 (2002)
132. F. Kneller, F.E. Luborsky, J. Appl. Phys. **34**, 656 (1963)
133. H. Pleifer, Phys. Status Solidi A **118**, 295 (1990)
134. G.I. Frolov, O.I. Bachina, M.M. Zav'yalova, S.I. Ravochkin, Tech. Phys. **53**, 1059 (2008)
135. F.C. Fonseca, G.F. Goya, R.F. Jardim, R. Muccillo, N.L.V. Carreño, E. Longo, E.R. Leite, Phys. Rev. B **66**, 104406 (2002)

136. J.M. Vargas, W.C. Nunes, L.M. Socolovsky, M. Knobel, D. Zanchet, Phys. Rev. B **72**, 184428 (2005)
137. S.V. Vonsovskii, *Magnetism* (Wiley, New York, 1974)
138. P. Langevin, Ann. Chem. Phys. **5**, 70 (1905)
139. I.S. Jacobs, C.P. Bean, in: *Magnetism III,* ed by G.T. Rado, H. Suhl (Academic Press, New York, 1963)
140. K. O'Grady, A. Bradbury, J. Magn. Magn. Mater. **39**, 91 (1994)
141. I.I. Yaacob, A.C. Nunes, A. Bose, J. Colloid Interface Sci. **171**, 73 (1995)
142. N. Moumen, M.P. Pileni, Chem. Mater. **8**, 11128 (1996)
143. J.C. Bacri, R. Perzinski, D. Salin, V. Cabuil, R. Massart, J. Magn. Magn. Mater. **62**, 36 (1986)
144. R.W. Chantrell, J. Popplewel, S.W. Charles, IEEE Trans. Magn. **MAG-14**, 975 (1978)
145. M. Stefanescu, C. Caizer, M. Stoia, O. Stefanescu, Acta Mater. **54**, 1249 (2006)
146. A.F. Pshenichnikov, W.V. Mekhonoshin, A.V. Lebedev, J. Magn. Magn. Mater. **161**, 94 (1996)